The winds are twisting: analysis of strong directional shear across the rotor plane using coastal lidar measurements and ERA5

Christoffer Hallgren[1,*], Heiner Körnich[2], Stefan Ivanell[1], Ville Vakkari[3,4], and Erik Sahlée[1]

[1]Department of Earth Sciences, Uppsala University, Uppsala, Sweden
[2]Swedish Meteorological and Hydrological Institute, Norrköping, Sweden
[3]Finnish Meteorological Institute, Helsinki, Finland
[4]Atmospheric Chemistry Research Group, Chemical Resource Beneficiation, North-West University, Potchefstroom, South Africa

Correspondence: Christoffer Hallgren (christoffer.hallgren@geo.uu.se)

Abstract. The change of wind direction with height (the directional shear) affects both the power production from a wind turbine, wake effects and aerodynamic loading. In this study, a climatology of the relative occurrence of strong directional shear over Scandinavia is created using 43 years of hourly ERA5 data covering the height range of a modern wind turbine and at wind speeds of operation. It is shown that strong directional shear ($\geq 15°$ over the rotor) is occurring 20–30% of the
5 time over land and 10–25% of the time over the extended Baltic Sea. The height of the atmospheric boundary-layer and the wind speed at hub height are identified as the most important predictors for strong directional shear, with low boundary-layer heights and weak winds being the main causes. Associated with this, a strong land–sea seasonality is observed. Furthermore, ERA5 is validated against lidar soundings from two coastal sites, both indicating a major underestimation in the distribution of the directional shear in ERA5. Especially in strongly stratified boundary-layers ERA5 struggles, with 25% of the data having
10 errors exceeding 24° and 28° for Östergarnsholm and Utö respectively.

1 Introduction

With advancing technology it has become more cost efficient to construct larger wind turbines, both onshore and offshore (e.g., Veers et al., 2019; Barthelmie et al., 2020; Duffy et al., 2020; Kumar et al., 2021). The pioneering onshore turbines in the 1990's had a typical rotor diameter of 50 m, increasing to 80 m in the 2000's, to 100 m in the 2010's and recently reaching beyond

15 120 m (US Department of Energy, 2022). Offshore, the evolution has been similar although turbine dimensions usually are much larger than onshore. The International Energy Agency (IEA) 15-MW reference offshore turbine (Gaertner et al., 2020) has a diameter of 240 m with blades sweeping from 30 to 270 m above sea level. In the advanced future offshore scenario by the National Renewable Energy Laboratory (NREL) it is possible to have 18-MW turbines with a rotor diameter reaching beyond 260 m already within the next few years (Vimmerstedt et al., 2022).

20 The large area covered by the rotor also implies that wind turbines are exposed to a great variation of meteorological conditions both horizontally and vertically across the rotor, such as changes in wind speed (e.g., Kettle, 2014; Møller et al., 2020; Debnath et al., 2021; Aird et al., 2022; Hallgren et al., 2022; Foody et al., 2023), wind direction (Kalverla et al., 2017;

Englberger and Lundquist, 2020), temperature (e.g., Janzon et al., 2020; Gadde and Stevens, 2021) and turbulence intensity (Türk and Emeis, 2010; Svensson et al., 2019; Bodini et al., 2020). These factors impact not only the performance and power production of a single wind turbine, but also the behaviour of the wake behind the turbine and thus the power production form the wind farm as a whole. For example, with the presence of a local wind speed maximum at a low height in the vertical profile, commonly referred to as a low-level jet (LLJ), the recovery of the wake can be faster compared to a reference case (Gadde and Stevens, 2021). These factors also influence the fatigue loads and longevity of the turbines. Robertson et al. (2019) showed that turbulence intensity and the change of wind speed with height, i.e., the wind shear, are key parameters in determining turbine loads, in combination with yaw (mis)alignment. Furthermore, the change of wind direction with height, i.e., the directional shear, is a secondary parameter that is relevant for turbine loads and a factor that also affects wake behaviour. In an observational study, Bodini et al. (2017) showed that under influence of directional shear, the vertical stretch of the wake manifests differently for the inner wakes, i.e., within a wind farm, as compared to the outer wakes, i.e., wakes from the edge of a row of turbines). We use the terminology directional shear throughout this article instead of veer, which is a standard notation in the wind industry, due to that it sometimes is confusing from a meteorological perspective where one separates between veering and backing winds due to the direction of the turning with height. With directional shear we here describe the change of wind direction with height, no matter if it is in the clockwise or anti-clockwise direction.

Although, there have been several publications in recent years on directional shear and its effect on wind power production, there is still an information gap when it comes to quantifying how often directional shear of different magnitude occurs in different regions. In an observational study from central Iowa, Sanchez Gomez and Lundquist (2020) showed that there was a pronounced connection between directional shear and low wind speeds and that directional shear exceeding $0.2°\,\mathrm{m}^{-1}$ was not uncommon in weak winds. For the US Atlantic coastal zone, Bodini et al. (2019) showed that there is a strong seasonality in directional shear, with higher shear values more likely to occur in summer.

Changes in the vertical profile of wind direction within the lowest 300 m of the atmosphere can be due to many different causes (Brown et al., 2005; Lindvall and Svensson, 2019). Under ideal conditions, and with a balance of the turbulent surface drag, the pressure gradient force and the Coriolis force, the wind turns up to 45° with height in the atmospheric boundary-layer. The rotation is clockwise in the Northern Hemisphere. This turning of the wind is often referred to as the (atmospheric) Ekman spiral (see e.g., Ekman, 1905; Englberger and Dörnbrack, 2018, for more details). Depending on the atmospheric stability, the turning of the wind often reduces to 15–40° (Svensson et al., 2016; Kalverla et al., 2017). On the synoptic scale, frontal systems can make the winds turn with height (e.g., Browning and Monk, 1982), associated with rapid changes in the properties between air masses. Among mesoscale phenomenon affecting the directional shear are the sea and land breeze circulations (Simpson, 1994; Miller et al., 2003; Hallgren et al., 2023), convective cells with a high degree of turbulent motions (Clarke, 1970; Svensson et al., 2017; Sanchez Gomez and Lundquist, 2020), non-ideal wind speed profiles (Kalverla et al., 2017; Hallgren et al., 2022), and internal boundary-layers in, e.g., the coastal zone or over forested areas (Hsu, 1979; Arnqvist et al., 2015). Also, topography induced directional shear can occur, such as e.g., katabatic winds and channeling in terrain with a high degree of complexity (Rotach et al., 2008; Heinemann and Zentek, 2021; Liu and Stevens, 2021).

A climatology that accurately describes the wind conditions is of high importance when planning for future wind power installations. Reanalysis data, see Sect. 2.1 for a description, are often used to create such climatologies. However, several studies have shown that reanalyses struggle resolving both the wind speed profiles (see Gualtieri 2022 for a review and also e.g., Hallgren et al. 2020 for details for the Baltic Sea and Kalverla et al. 2020 for the North Sea) and wind direction profiles (Brown et al. 2005 for the North Atlantic; Kalverla et al. 2020 for the North Sea; Lindvall and Svensson 2019 for onshore sites globally). Both onshore and offshore, reanalyses underestimate the turning of the wind with height, especially in stable stratification, with errors exceeding 30° (Brown et al., 2005; Lindvall and Svensson, 2019). Kalverla et al. (2020) showed that for the North Sea, recent wind atlases underestimate the occurrence of strong directional shear, exceeding the 95th percentile of the observations, relating this to the models' inability to properly account for mixing in case of stable stratification or strong baroclinicity. For an overview of different problems numerical weather prediction (NWP) models face in stable conditions, we refer to Holtslag et al. (2013) and Sandu et al. (2013).

In this study we analyse the directional shear in the Baltic Sea area, see Fig. 1a, focusing on the offshore conditions. Both observations and reanalysis data are investigated, generating a climatology of directional shear that could possibly be used to identify problematic areas for offshore wind energy development and areas where more focused measurement campaigns should take place for further investigations. The Baltic Sea is located at a high latitude and is a semi-enclosed sea with a relative short distance, maximally 150 km, to the nearest coastline from anywhere in the basin. As such, pronounced land-sea interaction processes are common, highly influencing the offshore wind conditions (e.g., Hallgren et al., 2020; Wu et al., 2020; Li et al., 2021; Rubio et al., 2022). The shallow sea, with an average depth of only 54 m, and the long coastline lowers the cost for connecting to the electrical grid, and the many countries neighbouring the sea combine to make the Baltic Sea a highly attractive area for wind power production. Projections from COWI (2019) and Wind Europe (2021) indicate a rapid increase from 2.2 GW installed capacity in 2020 to 93 GW in 2050. Onshore, Scandinavia is characterized by forests in large parts of Sweden and Finland, mountainous terrain in Norway and croplands in most of the rest of the domain shown in Fig. 1a.

To disentangle the mechanisms behind strong directional shear over the rotor plane of a wind turbine located in the Baltic Sea area and to evaluate and validate the performance of a state-of-the-art reanalysis, a combination of data from the fifth generation European Centre for Medium-Range Weather Forecasts (ECMWF) Reanalysis (ERA5) and multi-year Light Detection and Ranging (lidar) vertical profile observations of the wind speed and direction from two coastal sites in the Baltic Sea (Östergarns-holm and Utö, locations marked in Fig. 1b) is used. Although primarily analyzing and discussing the offshore and coastal conditions over the Baltic Sea area in this study, also onshore conditions are presented in the figures but are discussed in less detail.

2 Material and methods

To obtain a climatology of directional wind shear and search further understanding of the steering mechanisms behind strong directional shear, observations of the wind profile are needed. However, since this type of measurements are sparse and typically not covering more than just a few years, they need to be supplemented with gridded model data, covering multiple decades
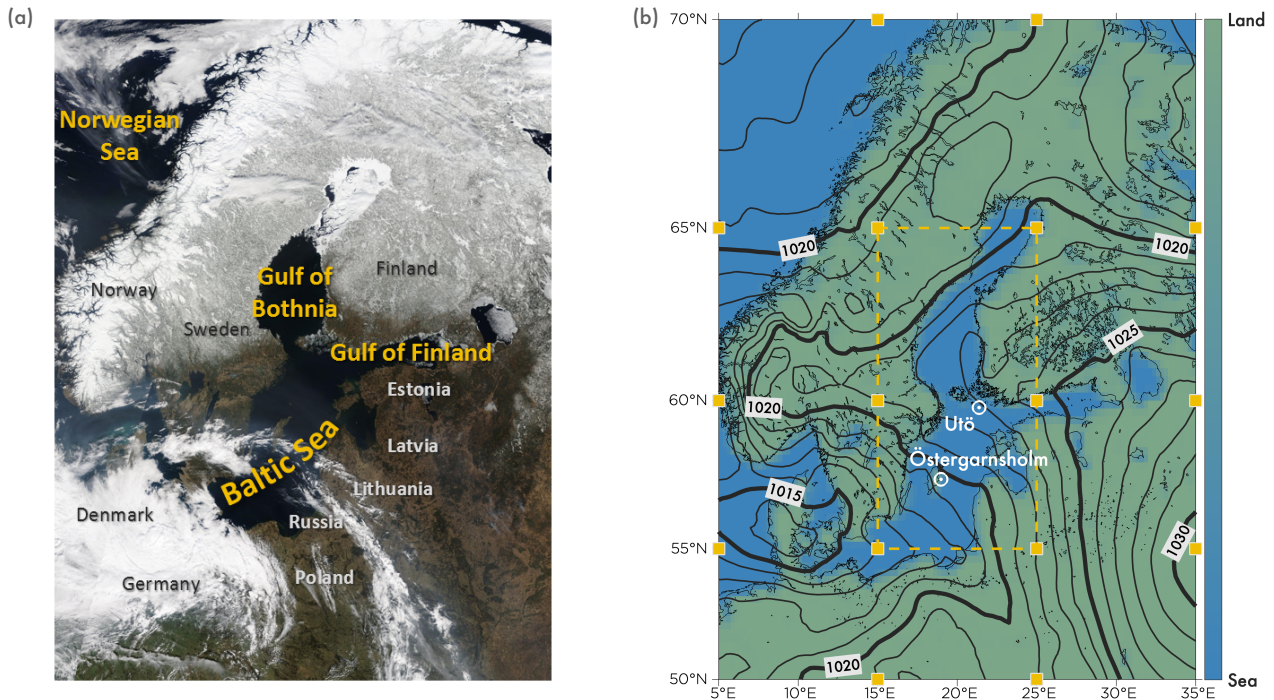
Figure 1. In panel (a) a satellite image of the Baltic Sea area is shown with labels for the different parts of the basin and on the surrounding countries. In panel (b) the land/sea-mask from ERA5 is shown in green/blue and the sites where lidar observations of the wind profile are performed, Östergarnsholm and Utö, are marked. The layout of the sixteen grid points used for the synoptic weather classification are marked in the map (yellow squares, see Sect. 2.5 for details) and the focus area of the classification is marked with the dashed yellow line. The satellite image in panel (a) and the sea level pressure field in panel (b) are from 14 April 2018, 12 UTC (the same date and time as for the Utö wind profiles in Fig. 2c). We acknowledge the use of satellite imagery in panel (a) from the Worldview Snapshots application (https://wvs.earthdata.nasa.gov), part of the Earth Observing System Data and Information System (EOSDIS).

90 allowing for a larger statistical sample. For the overlapping time period, and for the grid point closest to the location of measurements, the model can be validated against the measurements, identifying systematic errors in the model.

In this section, the reanalysis model ERA5 and the lidar observations are presented, followed by a description of the method applied to calculate the maximum directional shear over the rotor plane of a wind turbine. Furthermore, the classifications of non-ideal wind speed profiles and synoptic weather conditions used to investigate the occurrence of strong directional shear

95 are presented. This is followed by a description of the statistical method that was used to calculate the importance of different variables as indicators of strong directional shear.

2.1 ERA5

A reanalysis is an optimized gridded description of the state of the atmosphere at a specified point in (the past) time. With three-dimensional reanalyses, spanning multiple decades it is possible to study short-lived events as well as creating climatologies.
ERA5 is a state-of-the-art global reanalysis with a horizontal resolution of $0.25° \times 0.25°$, corresponding to approximately 17 km $\times$ 31 km in the Baltic Sea area, and a temporal resolution of 1 hour. In the vertical, 137 hybrid sigma levels are applied, of which 10 levels are in the lowest 300 m above sea level in the standard atmosphere (Hersbach et al., 2020). Using a wide range of different types of weather observations, covering both direct measurements and remote sensing, the ECMWF Integrated Forecasting System (IFS) model is applied to perform the data assimilation. In this study, we analyze hourly ERA5 data covering the time period 1979–2021. Although ERA5 data is available back to 1940, the reanalysis is known to be of higher quality from 1979 onward, as this year marks the start of the modern era, with sufficient availability of satellite data to significantly improve the reanalysis (Bell et al., 2021).

From the eastward and northward components of the wind at the ERA5 model levels, the wind speed and direction were calculated at each level, and from the surface pressure, the profiles of temperature and specific humidity the heights of the levels were calculated. In addition to this, the 2-m temperature (T2m), the total amount of large-scale and convective precipitation (precip.), the proportion of low cloud cover (LCC), and the boundary-layer height (BLH) were obtained and analysed in terms of importance of predicting strong directional wind shear. The BLH in ERA5 is calculated based on the bulk Richardson number, following the conclusions from the review by Seidel et al. (2012, see also Vogelezang and Holtslag 1996), and is thus strongly linked to the stability of the boundary-layer. The BLH is set to be the height where the bulk Richardson number reaches the critical value of 0.25 and within the boundary-layer, the bulk Richardson number has a lower value than 0.25, implying (dynamically) unstable conditions that are or, can easily become, turbulent.

2.2 Lidar observations

The vertical profile of wind speed and direction was measured using lidar instrumentation at two coastal sites in the Baltic Sea; Östergarnsholm and Utö, see Fig. 1b. Below, details are presented about the sites and their respective instrumentation.

2.2.1 Östergarnsholm

About 3 km east of the island of Gotland, the smaller island Östergarnsholm is located (57.43 N, 18.98 E) in the central parts of the Baltic Sea. Östergarnsholm is a rather flat island with an area measuring approximately 1 km^2. At the very southern tip of the island, a meteorological research station (Rutgersson et al., 2020) is located and among the instrumentation was a ZephIR 300 wind lidar (ZX Lidars) during the period December 2016 – June 2020. The lidar was set to measure the wind profile at 28, 39, 50, 100, 150, 200, 250 and 300 m above mean sea level. As the lidar measures the wind using a continuous-wave laser beam, this implies that the extent of the measurement volume grows rapidly with height. Assuming no beam attenuation and a homogeneous distribution of backscatter elements in the boundary-layer, a Cauchy–Lorentz distribution (following Mann et al. 2010, see also Svensson et al. 2019) was used to estimate that 50% of the backscatter at 100 m was within ±8.9 m and within

±80 m at 300 m height. Measurements were stored with 10 min intervals, but for comparison with the ERA5 data in this study,
130   only the average wind speed and direction from the 10 min period at the full hour was used.

The main direction of the wind was measured at the instrument itself, at approximately 1 m above the surface, and deviations from this wind direction in the profile were recorded. This implies that in weak wind conditions, with a high degree of stochastic variation of the wind direction, and in cases of winds from the sector 110–150°, where a nearby hut was partly sheltering the wind at the lowest 0–3 m above the surface, there could be an erroneous classification of the main wind direction (Svensson
135   et al., 2019). However, these occasions were not considered problematic, as it is the difference in wind direction in the 30–270 m layer and at wind speeds exceeding $3 \, \mathrm{m \, s^{-1}}$ that is the main objective of this study, see Sect. 2.3 for details. In general, winds from the sector 45°—220° represents pure open sea conditions. For winds from the 220°--295° sector the properties of the advected air is influenced by Gotland and from the 295°–355° sector, Östergarnsholm affects the flow, further details in Rutgersson et al. 2020 and Hallgren et al. 2022).

140   In Fig. 2a, an overview of the availability of the Östergarnsholm lidar data is presented. The lidar was moved for testing at another site 23 January – 29 April 2019 and for service at the manufacturer 11 August – 2 December 2019. As a complement to the built-in quality control by the manufacturer, an additional quality control was applied to remove spikes in the wind speed and wind direction profiles and also of profiles with less than 75% data availability. Furthermore, all profiles with extremely strong directional shear over the rotor, see Sect. 2.3, were manually examined. In total, these additional steps in the quality control
145   led to a removal of 16.2% of the lidar data. Lidar observations from Östergarnsholm have been used in earlier studies both for validation of measurements of the wind speed and direction comparing with a 30 m meteorological tower at the research station (Svensson et al., 2019), validation of different reanalyses (Hallgren et al., 2020) and in analyses of the occurrence of non-ideal wind speed profiles (Hallgren et al., 2022). For a more thorough description of the site and all other measurements performed at Östergarnsholm, we refer to Rutgersson et al. (2020).

150   **2.2.2 Utö**

Utö (59.78°N, 21.37°E) is located approximately 300 km northeast of Östergarnsholm and 60 km off of the Finnish mainland. The area of the island is $0.81 \, \mathrm{km^2}$ and the highest point reaches 16 m a.s.l.. Utö is situated at the southern edge of the Finnish archipelago with the two nearest islands of comparable size approximately 12 km to the west and northeast, respectively. A Halo Photonics Stream Line scanning Doppler lidar is located on top of a container at 8 m a.s.l. at the atmospheric research
155   station (Hirsikko et al., 2014; Laakso et al., 2018). The lidar was upgraded to the XR version laser and amplifier in October 2017.

The Halo Stream Line is a pulsed Doppler lidar capable of full hemispheric scanning. Here we utilize wind profiles from velocity azimuth display (VAD) scan at 15° elevation angle, which was configured with 24 azimuthal directions and scheduled to run every 15 minutes. Range resolution of the lidar is 30 m and lowest 90 m are discarded due to effects by outgoing pulse,
160   which results in 7.8 m vertical resolution from 35 m a.s.l. up. The radial measurements were post-processed according to Vakkari et al. (2019) and an SNR-threshold of 0.005 was applied to the radial data before wind retrieval, which was done with sinusoidal fitting (compare Browning and Wexler, 1968).
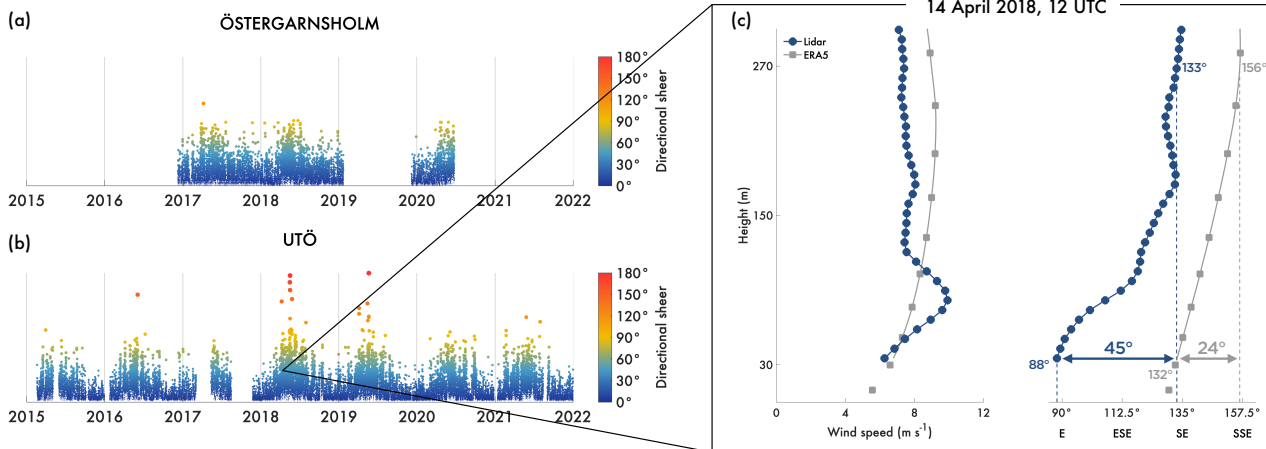
Figure 2. In panel (a), time series of directional shear over the rotor (30–70 m) for Östergarnsholm are plotted, and in panel (b) for Utö. The size and color coding of the data points is relative to the directional shear. Panel (c) shows an example of wind speed and wind direction profiles, lidar and ERA5, for Utö for 14 April 2018, 12 UTC and the maximum directional shear over the rotor of the IEA 15-MW offshore reference turbine (Gaertner et al., 2020) for both the lidar and ERA5 is printed.

The bearing angle of the lidar was verified by scanning across the sector of the old lighthouse located 370 m northwest of the lidar. The scan was configured with a low elevation angle and high azimuthal resolution to ensure that the beam hits the lighthouse, which enables determining the bearing angle of the lidar at better than 1° precision. In atmospheric measurements, instrumental noise, turbulence and local effects distort observed radial wind from the ideal sinusoidal curve (e.g. Vakkari et al., 2015). Bootstrapping was used to estimate the combined effect of all sources of uncertainty in both wind speed and direction retrievals.

In the analysis, the Utö lidar data was limited to 300 m a.s.l.. To extract data at the full hour the wind speed was linearly interpolated temporally and the wind direction at the closest time step was used, in both cases allowing a maximum gap of 60 minutes. This was performed individually for each height level. As for the Östergarnsholm lidar, data from the Utö lidar also underwent additional quality control and profiles with less than 75% data availability and profiles with spikes were removed. Manual quality control was performed on profiles indicating extreme directional shear. In total 3% of the data was removed in the quality control. Data availability for the Utö lidar is presented in Fig. 2b.

2.3 Maximum directional shear over the rotor

In this study we consider the maximum change of wind direction over the rotor of the 15-MW offshore reference turbine (Gaertner et al., 2020) at wind speeds of operation. In other words, the maximum directional shear is defined as the maximum change of wind direction considering all heights with data, lidar observations or reanalysis, in the range 30–270 m when the wind speed at hub height (150 m) was between 3 m s^{-1} (cut-in) and 25 m s^{-1} (cut-out). To simplify comparisons between

onshore and offshore conditions, the same turbine type was applied in the full domain, as the main focus is to study offshore conditions.

For a fair comparison between ERA5 and lidar observations, the ERA5 wind components on model levels were interpolated to match the measurement heights of the lidar by fitting a Piecewise Cubic Hermite Interpolating Polynomial (PCHIP) on a logarithmic height scale to the wind components in the profile, independently. The wind speed and wind direction were then calculated. For Utö, the wind speed at hub height (150 m) was assumed to be the same as the wind speed on the closest measuring height (151.6 m) as measured by the lidar. For Östergarnsholm measurements at 150 m were in the original lidar data. The directional shear was categorized as strong if the wind turned 15° or more within the vertical span of the rotor, as very strong shear if the wind turned 30° or more, or as extreme shear if the wind turned 45° or more. An example of extreme directional shear is shown in the Utö lidar measurements, from 14 April 2018. 12 UTC, in Fig. 2c, where the wind turned from 88° (E) at the bottom of the rotor to 133° (SE) at the top of the rotor. Note that in this work, only the magnitude of the change of the wind direction with height is considered, not if the turning is clockwise (veering winds) or anti-clockwise (backing winds). Also, note that if there is a local maximum or minimum in the wind direction profile, i.e. if the wind is veering/backing up to some height, and then is backing/veering higher up, it is still only the maximum change in wind direction over the rotor that is considered.

2.4 Non-ideal wind speed profiles

In contrast to ideal wind speed profiles where the wind speed is increasing with height, non-ideal profiles, such as LLJs (profiles with a pronounced local maximum), profiles with a local low-level minimum (LLM), and profiles with decreasing winds with height (negative profiles), are common over the Baltic Sea, especially in spring and summer (Hallgren et al., 2022). Following the definitions applied by Hallgren et al. (2022), a wind speed profile is classified as a strong LLJ if the decrease in wind speed above the local maximum, i.e., the fall-off above the jet core, is exceeding both 2 m s^{-1} and 20% of the wind speed at the core. Similarly, a profile is classified as a weak LLJ if the fall-off is exceeding 1 m s^{-1} and 10% of the core speed, but was not classified as a strong LLJ. Transition profiles are profiles with a very weak local maximum and can be considered as transition states between ideal profiles and weak LLJs, fulfilling that the falloff is exceeding 0.5 m s^{-1} and 5% of the core speed and that the profile is not already classified as either a weak or a strong LLJ. LLMs occur when the wind speed profile exhibits a local minimum and the increase in wind speed above the minimum is at least 1 m s^{-1} and 10% of the speed at the local minimum. Profiles where the wind speed decrease by at least 1 m s^{-1} up to 300 m, comparing the maximum and minimum wind speeds in the profile, are classified as negative given that the profile was not already classified as a weak or strong LLJ, a transition profile or an LLM. For both negative profiles and LLMs, note that, as the wind speed goes to zero at the surface, this implies that there has to be a local maximum in the wind speed somewhere between the surface and the lowest level of lidar measurements. Profiles that were not classified as any of the non-ideal types were considered to be ideal. Note however that also these profiles can display a local minimum or maximum or could have slight negative shear, as long as they are not fulfilling the criteria for any of the non-ideal profiles. For more details on the properties of these different types of profiles and when they occur, we refer to the observational study using lidar data from Östergarnsholm by Hallgren et al. (2022).

2.5 Synoptic weather classification

215 To classify the synoptic conditions over the Baltic Sea, the objective Jenkinson and Collison (1977) method to identify the prevailing Lamb Weather Type (LWT) was applied (Lamb 1972, see also Jones et al. 2012 and Fernández-Granja et al. 2023). LWTs have been used for many different applications and in terms of offshore/coastal wind conditions, we refer to Kalverla et al. (2019) for a study of LLJs over the North Sea, to Hallgren et al. (2023) for a study of the occurrence of sea and land breezes along the coast of southern Sweden and to Hallgren et al. (2021) for an analysis of different post-processing methods 220 to improve coastal wind power production forecasts using Utö lidar data.

Based only on the ERA5 sea level pressure at sixteen grid points, located as marked in Fig. 1b, the synoptic vorticity, wind speed and direction representative for a focus area, also marked in Fig. 1b, was calculated, hour by hour for the period 1979–2021. This information was then used to classify the synoptic conditions for every hour into one of the 27 LWTs. If the flow was purely anti-cyclonic without any dominant wind direction, the synoptic conditions were categorized as A. Similarly, 225 for cyclonic situations, the conditions were categorized as C. In cases with low synoptic vorticity, but with a dominant wind direction, the LWT was given by one of the eight cardinal wind directions (N, NE, E, ...). Similarly, in cases with stronger synoptic vorticity in combination with a dominant wind direction, the LWT was categorized as AN, ANE, AE, ... in anti-cyclonic cases or as CN, CNE, CE, ... in situations with cyclonic vorticity. In case of weak synoptic flow, with a low degree of vorticity, the LWT was denoted U. As an example in the case of 14 April 2018, 12 UTC, the LWT was classified as S, see Fig. 230 1b.

2.6 Calculation of predictor importance

To better understand which are the driving mechanisms behind strong directional shear, >15°, we investigate a selection of eight variables: the BLH, the wind speed at hub height (ws150), the wind direction at hub height (wdir150), the T2m, the LWT, the LCC, the precip., and the shape of the wind speed profile (Profile Type). Among these the BLH, the ws150, the wdir150, 235 the T2m, the LCC, and the precip. are continuous variables, while the LWT and the Profile Type are categorical variables. The variables are selected on the basis of being known to affect the wind profile at heights relevant for wind power, having low cross-correlation (which simplifies analysis of their importance), and/or easily being measured at a meteorological station. As the wind speed and wind direction at hub height are not directly provided in ERA5, the wind components were interpolated to 150 m as described in Sect. 2.3.

240 To calculate the importance of the different variables when it comes to predicting strong directional shear, a binary classification tree was fitted to 43 years of hourly ERA5 data (1979–2021) for the grid points closest to Östergarnsholm and Utö, 7.8 and 7.7 km away respectively. The decision tree was set up using a uniform cost matrix; having the same cost for falsely classifying an hour as having strong directional shear as missing to predict an hour with strong directional shear. Empirical data for the prior probability of occurrence of strong shear was used and at each split in the tree the predictor that minimized 245 the p-value of the χ^2-test of independence between each predictor and the response was chosen (Shih, 1999). The predictor

importance was then derived by estimating the risk at each branch split in the tree. Finally, the relative importance of each of the predictors was calculated, summing up to 100%.

3 Results

3.1 ERA5 climatology of directional shear in the Baltic Sea area

250 In Fig. 3, the relative occurrence of the ERA5 maximum directional shear over the rotor exceeding 15°, 30°, and 45° for the Baltic Sea region is shown, based on the period 1979–2021. In general, there was a major difference between land and sea in the relative occurrence of strong directional shear, with the highest frequency of occurrence over land. In the greater part of Finland and in northeastern Sweden, strong directional shear occurred more than 30% of the time and in general 20–30% of the time for other onshore areas. Offshore and in coastal waters, strong directional shear typically occurred 0–20% of the time,
255 the further offshore the lower the frequency, see e.g., the Norwegian Sea. The highest occurrence of strong directional shear over water was found in the Bay of Bothnia and locally along the Swedish east coast as well as over the big lakes.

For most of the Baltic Sea region, very strong directional shear was rare, but mainly occurred in northeastern Sweden, northwestern Finland and in the northern parts of Norway, on average 5–10% of the time for the 43 years analysed. However, in Norway, the relative occurrence locally reached 15%, possibly related to the sharp transition from ocean to mountains in
260 this area. Naturally, it is also in this region that extremely strong directional shear occurs most frequently, locally up to almost 5% of the time. Onshore along the coast of northern Sweden, extremely strong directional shear was occurring approximately 2–3% of the time.

As seen in Fig. 4, there was a clear seasonality in the occurrence of strong directional shear both onshore and offshore. In the fall and winter period (September to February, Fig. 4a), strong directional shear was mainly occurring over land, up to 40–50%
265 of the time in most of northern Scandinavia. Offshore, strong directional shear was occurring less than 10% of the time for these seasons (fall and winter). In spring and summer (March to August) the pattern changed, see Fig. 4b. The differences in relative occurrence of strong directional shear between land and sea is less pronounced with strong directional shear occurring 10–40% of the time in general. However, areas where strong directional shear was most common were all located in the extended bays of the Baltic Sea, including the Bay of Bothnia and the Gulf of Finland. In these areas, the 15° threshold was exceeded 30–40%
270 of the time.

3.2 Predictor importance for strong directional shear

By fitting a binary classification tree, see details in Sect. 2.6, to 43 years of single-level ERA5 data for the grid point closest to Östergarnsholm and Utö, respectively, the relative predictor importance for strong directional shear was calculated, see Fig. 5a. The same pattern was seen for both sites as the BLH stood out as the most important predictor, followed by the ws150,
275 the wdir150 and the T2m. Lower predictor importance was seen for the LWT, the LCC, the precip., and the shape of the wind speed profile. In Fig. 5b–e, scatter plots based on the ERA5 data show the relation between directional shear and the four most
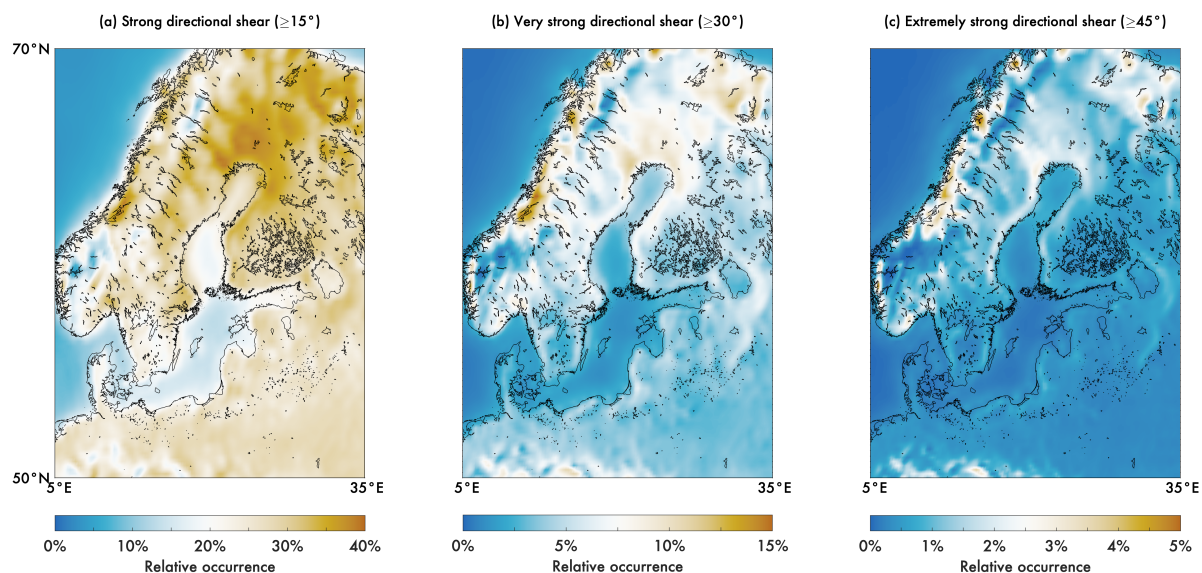
Figure 3. Relative occurrence of maximum directional shear over the rotor exceeding (a) 15°, (b) 30°, and (c) 45° for the Baltic Sea area. Note that the same vertical extent of the rotor, assuming the IEA 15-MW reference turbine (Gaertner et al., 2020), was applied both onshore and offshore. The climatology is created from hourly ERA5 data for the period 1979–2021.
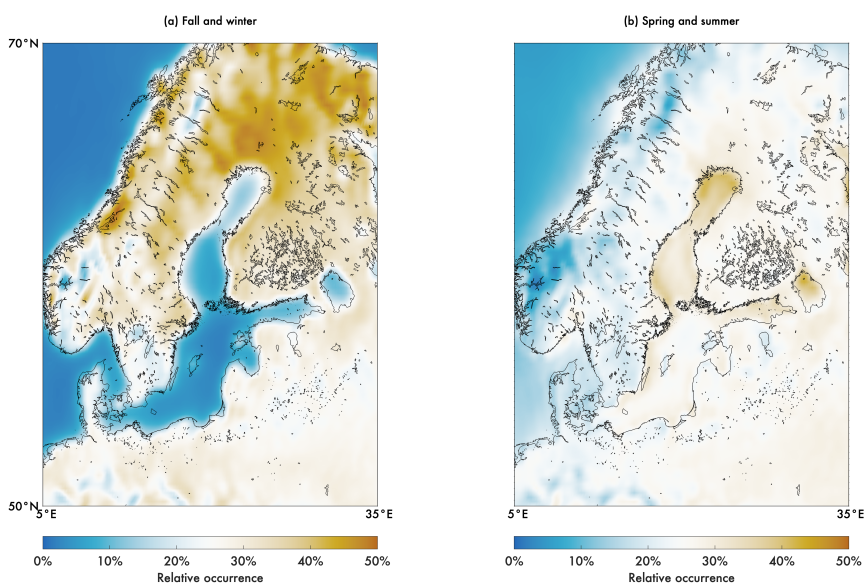
Figure 4. Relative occurrence of maximum directional shear over the rotor exceeding 15° in (a) fall and winter (September to February) and (b) spring and summer (March to August) for the Baltic Sea. Note that the same vertical extent of the rotor, assuming the IEA 15-MW reference turbine (Gaertner et al., 2020), was applied both onshore and offshore. The climatology is created from hourly ERA5 data for the period 1979–2021.

.

important predictors: the BLH (Fig. 5b), the ws150 (Fig. 5c), the wdir150 (Fig. 5d), and T2m (Fig. 5e) for both Östergarns-holm and Utö. In Table 1 the median values of the distributions of BLH, ws150 and T2m are presented for cases of strong, very strong and extremely strong directional shear. Using the Wilcoxon rank sum test (Mann-Whitney U-test), it was shown that the medians for all three categories of directional shear were significantly different from each other at the 95% confidence level, apart from the medians for T2m in case of very strong och extremely strong directional shear for both Östergarnsholm and Utö, where no difference was ascertained. Note that, although one of the most important predictors, wdir150 was not included in this analysis as the coordinates for that variable are circular, and thus the test is not applicable.

Starting with the BLH, Fig. 5b, almost all occasions with strong directional shear, >15°, occurred at BLHs lower than 500 m, cases of very strong directional shear, >30°, at BLHs lower than 270 m (the top height swept by the turbine blades), and extremely strong directional shear, >45°, at BLHs lower than 150 m (hub height). In general, the lower the BLH, the stronger the directional shear, and there is a significant difference between the medians of the distributions for all three levels of directional shear, see Table 1. As the conditions typically are stable over the Baltic Sea in spring and early summer, implying a lower BLH, the scatter plots for the BLH also suggest some seasonality in the data (compare with Fig. 4), and this is further strengthened by the result in Fig. 5e where the distribution is shifted towards higher temperatures for cases with strong directional shear.

The wind speed at hub height, Fig. 5c, ranges from the 3 m s^{-1} cut-in wind speed to the 25 m s^{-1} cut-out wind speed, as a cause of the definition of directional shear over the rotor applied in this study, see Sect. 2.3. The shape of the distribution is similar to the what is seen for the BLH, Fig. 5b, and indicates that the highest values of directional shear tend to appear in the lowest wind speeds. For both Östergarnsholm and Utö, the major part of the distributions was between 5 and 10 m s^{-1} with directional shear values below 5°. Strong directional shear, exceeding 15°, was occurring in all wind speeds up to, in general, 17 m s^{-1} for Östergarnsholm and 18 m s^{-1} for Utö, with the most extreme cases at winds weaker than 5 m s^{-1}. Extremely strong directional shear typically only occur when the wind speed is just over cut-in, with the distribution centered around 3.6 m s^{-1} for both sites.

For both Östergarnsholm and Utö, winds directed from southwest are the most common. In general, the directional shear over the rotor is somewhat stronger when the wind is from this direction, however staying below the 15° threshold most of the time, see Fig. 5d. Strong directional shear can occur in any wind direction and there is no clear pattern in the distribution of the data, which was also suggested by the relatively low importance of the predictor in Fig. 5a. Similarly, the predictor importance for T2m, Fig. 5a, goes hand in hand with the distribution of data in Fig. 5e. As previously mentioned, strong directional shear was primarily occurring in relatively high temperatures, with medians of 10.6°C for Östergarnsholm and 8.7°C for Utö, probably connected to the lower BLH in coastal locations during summer and also to generally weaker winds during the hottest days. Neither for Östergarnsholm nor for Utö, any significant difference was found comparing the medians of the distributions of T2m in case of very strong or extremely strong directional shear, see Table 1.

The relatively low predictor importance for the LWT, the LCC, the amount of precipitation, and the shape of the wind speed profile is linked both to the variation of directional shear versus the variable and to the distribution of the variable itself. For example, although non-ideal wind speed profiles likely are linked to pronounced directional shear according to observations,
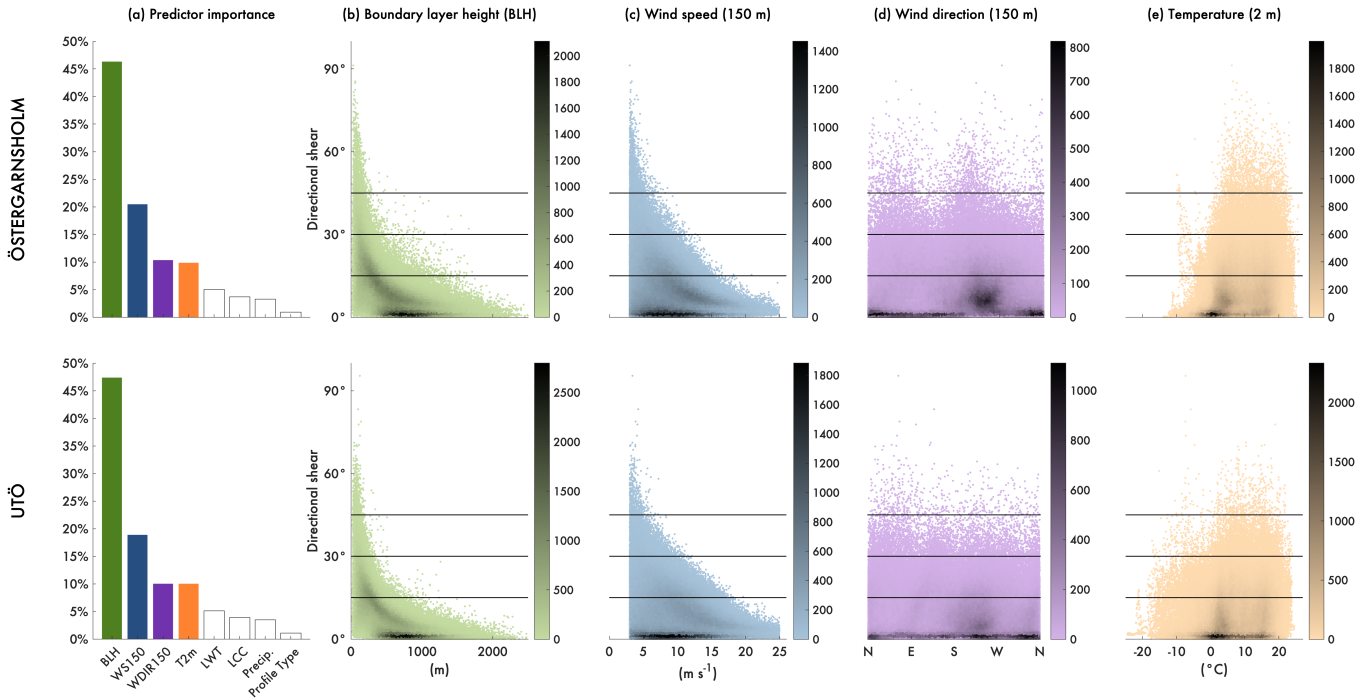
Figure 5. Predictor importance for strong directional shear, $\geq 15°$, in 43 years of ERA5 data (1979–2021) at Östergarnsholm (top row) and Utö (bottom row) for the eight selected variables (Sect. 2.6) is plotted in panel (a). The predictor importance was calculated using a binary classification tree (Sect. 2.6). In columns (b)–(e) scatter plots of directional shear versus the four most important predictors (BLH, ws150, wdir150, T2m) are shown, respectively. The horizontal lines at 15°, 30°, and 45° mark the thresholds for strong, very strong, and extremely strong directional shear. The density of the data in the scatter plots is indicated by the darkness of the colour, with black dots indicating the highest density. The number of counts (hours) that each dot represents is given by the colorbar.

Table 1. Median of the distributions of BLH, ws150 and T2m, see Fig. 5, in case of strong, very strong and extremely strong directional shear using hourly ERA5 data for the period 1979–2021 for the grid points closest to Östergarnsholm and Utö, respectively.

	Östergarnsholm			Utö		
	Strong (15°–30°)	Very strong (30°–45°)	Extremely strong ($\geq 45°$)	Strong (15°–30°)	Very strong (30°–45°)	Extremely strong ($\geq 45°$)
BLH (m)	224	120	86	197	103	78
ws150 (m s^{-1})	7.0	4.7	3.6	7.7	4.7	3.6
T2m (°C)	10.6	11.5	11.4	8.7	9.8	9.6

see Sect. 3.4, the relative occurrence of non-ideal wind speed profiles in ERA5 is so low that the importance of this as a predictor almost vanishes completely.

To investigate the spatial variation of the key predictor variable, BLH, the relative occurrence of BLH in different height bins is plotted for the two seasons (fall and winter, spring and summer) in Fig. 6a–h. For most onshore locations in the Baltic Sea area, the BLH in fall and winter was typically in the range 0–500 m, offshore the range 500–1000 m was the most common. In spring and summer, the BLH was most often in the height interval 150 – 500 m over the Baltic Sea, Fig. 6f, while it was equally distributed between the four bins onshore, see Fig. 6e–h.

Similarly, the second-most important variable, the ws150, was divided into four bins, 3–6, 6—9, 9–12, >12 m s^{-1}. The results clearly show that most data fell into the first bin in the mountainous area in Norway in both fall and winter, Fig. 6i, and in spring and summer, Fig. 6m. As weak winds are a good indicator of the strength of the directional shear, Fig. 5c, this explains part of the relatively high frequency of very strong, >30°, and extremely strong, >45°, directional shear in this area, see Fig. 3bc. Note however that the resolution in ERA5, $0.25° × 0.25°$, is not enough to resolve the complex terrain in the mountains accurately, and results for this region should be interpreted with extra care. Offshore, winds exceeding 12 m s^{-1} were most common in fall and winter, Fig. 6l, while all wind speed bins were approximately equally frequent offshore in spring and summer, Fig. 6m–p.

Although the synoptic weather conditions are not among the most important predictors for strong directional shear, analysis of the occurrence of directional shear in different LWT can still provide some insights in the physical mechanisms behind the formation of such profiles. In Fig. 7, five of the 27 LWTs are presented for the spring and summertime conditions together with the relative occurrence of strong directional shear in each class. All 27 LWTs for fall–winter and spring–summer with their corresponding relative occurrence of strong directional shear, are included in the supplement. Note that the focus area applied for LWT classification in this study was located over the Baltic Sea, Fig. 1b. As such, the validity of the classification decreases with increasing distance to the focus area. This is important to keep in mind when interpreting the maps of directional shear in different LWTs. The classification scheme is known to be prone to have a high relative frequency of pure anti-cyclonic flow (16.7% in the spring–summer seasons) and pure cyclonic flow (17.7%) while other LWTs generally are less frequent (compare e.g., with the numbers in Kalverla et al. 2019 for an ERA5 climatology of LWTs over the North Sea).

With a high pressure, LWT A, centered over the focus area, strong directional shear is common over the Baltic Sea, especially close to the coast. Under cyclonic conditions, LWT C, with a low-pressure centered in the focus area, the relative occurrence of strong directional shear is lower. As seen by the higher density of the isobars, indicating a sharper gradient in the pressure field for LWT C than in LWT A, the wind speed is also higher in cyclonic conditions, which in turn is linked to a lower directional shear, Fig. 5c. With a high pressure centered southwest of the focus area, the synoptic flow is from the northwest over the Baltic Sea, LWT ANW, occurring 1.4% of the time in spring and summer. In this case the air is advected over Sweden and then over the Baltic Sea, resulting in strong directional shear occurring approximately 30–50% of the time in offshore coastal areas along the Swedish east coast. For the Gulf of Finland, the air has been advected over Finland before entering over the water, and also there the change in surface properties results in a higher relative frequency of directional shear. Southwesterly winds, LWT SW, are dominating in the Baltic Sea region and it is visible that the change in surface conditions cause a higher
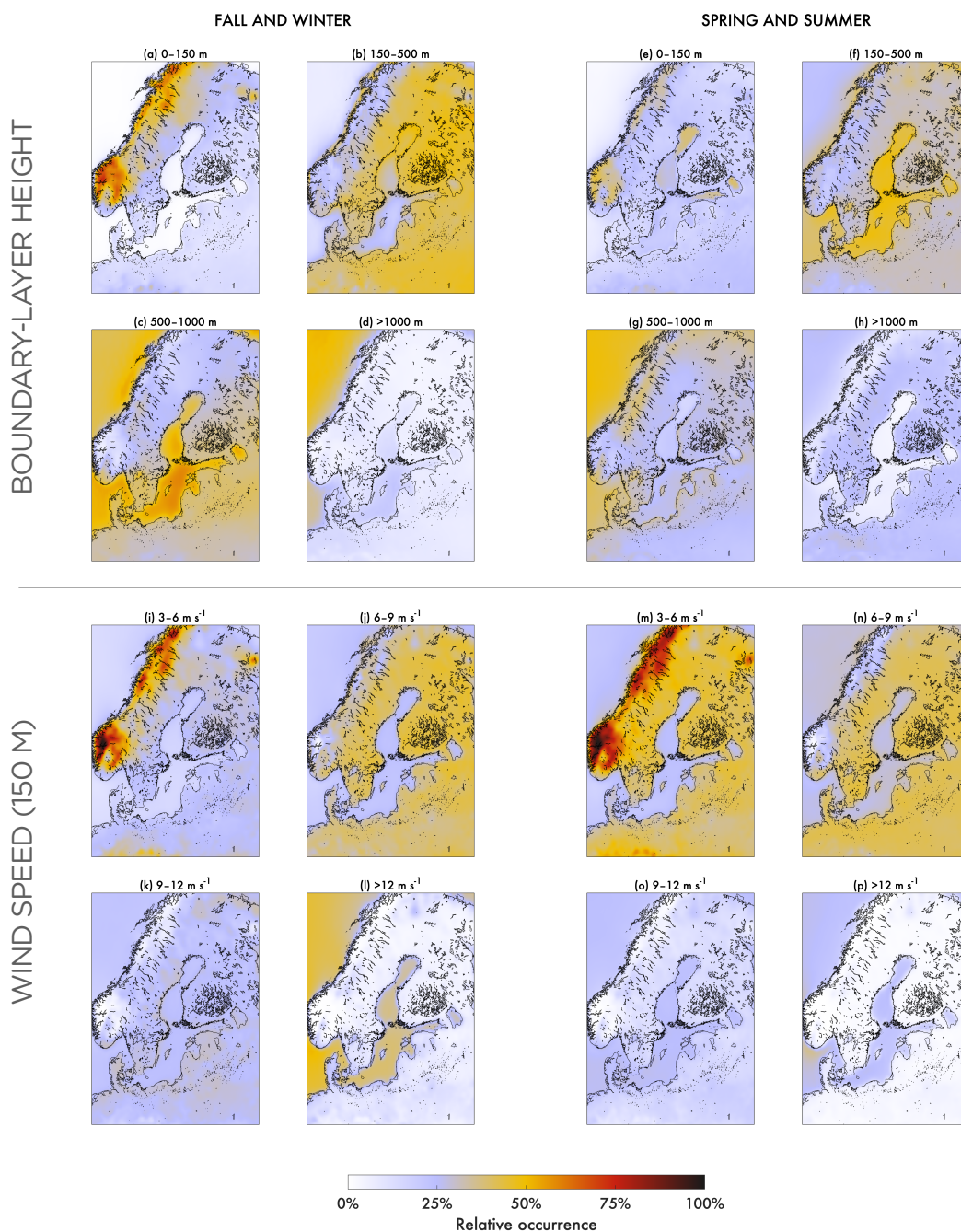
Figure 6. Top: relative occurrence of BLH in four different bins, 0–150, 150–500, 500–1000, >1000 m, for fall and winter (September to February) in panels (a)–(d) and spring and summer (March to August) in panels (e)–(h). Bottom: relative occurrence of wind speed at hub height (150 m) in four different bins, 3–6, 6—9, 9–12, >12 m s^{-1}, for fall and winter in panels (i)–(l) and spring and summer in panels (m)–(p). The climatology is created from hourly ERA5 data for the period 1979–2021.
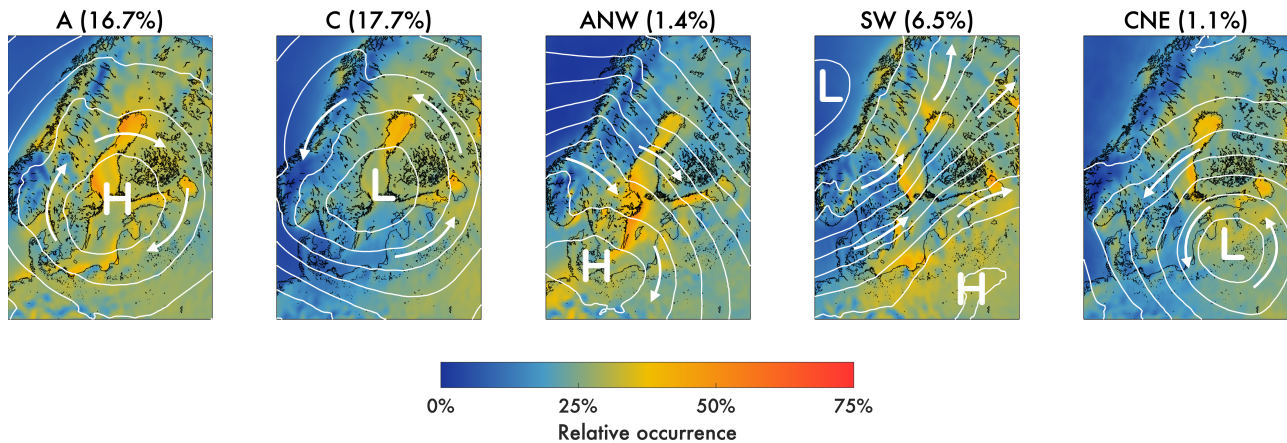
Figure 7. Relative occurrence of strong directional shear, ≥15°, in five selected LWTs based on hourly ERA5 data for the spring–summer seasons (March to August) in the period 1979–2021. The relative occurrence of each LWT is indicated. High pressure centers, H, and low-pressure centers, L, are marked in the panels, as well as isobars showing every 2nd hPa for the sea level pressure field, averaged in each LWT. Arrows indicate the approximate synoptic wind direction, but are not scaled with the wind speed. See Sect. 2.5 and Fig. 1b for details on the synoptic classification of the mean sea level pressure field into different LWTs. Similar maps for all 27 LWTs for both fall and winter, and spring and summer, are presented in the supplement.

degree of directional shear along the east coast of Sweden. Similarly, when the governing synoptic conditions are cyclonic with northwesterly winds, CNE, strong directional shear is prone to occur along the west coast of Finland, as the air is advected over Finland before reaching the coast.

3.3 Coastal observations of directional shear

350 In Fig. 2, time series of lidar measurements of directional shear over the rotor is plotted for Östergarnsholm (panel a) and Utö (panel b). As expected from the previous analysis of ERA5 data, a pronounced seasonality can be identified for both coastal sites, with generally higher values of directional shear in spring and summer than in fall and winter. For both sites, a few occasions of extreme conditions exceeding 60° directional shear was recorded every year. While there are some recordings of directional shear exceeding 90° in the Utö lidar time series, in the most extreme cases almost reaching the maximum possible

355 directional shear, 180°. Östergarnsholm was never exposed to such extreme conditions, according to the measurements.

On 14 April 2018, the maximum directional shear over the rotor was extremely strong at Utö, with a maximum of 95° at 3 UTC and a minimum of 32° at 15 UTC according to the lidar profile. At 12 UTC, see wind speed and wind direction profiles plotted in Fig. 2c, the directional shear was 45°, with winds turning clockwise with height (veering winds); from easterly winds, 88° wind direction, at the lower part of the rotor to southeasterly winds, 133°, in the top part. In ERA5, the directional

360 shear was modeled to be 24° at the grid point closest to Utö and at the same point in time. As evident from Fig. 2c, ERA5 did not only underestimate the strength of the directional shear by 21°, but also had an offset of approximately 20–40° from

the correct prevailing wind direction. The synoptic conditions, presented in Fig. 1a and b, indicated predominantly southerly winds over the Baltic Sea focus area as a consequence of the pressure field with a low-pressure centered over Denmark and a high pressure over Russia in the easternmost part of the map, and were classified as LWT S.

365   The Utö lidar wind speed profile was mostly classified as a strong LLJ throughout the day but oscillated to be classified as a weak LLJ for a few hours in the late morning and also in the late evening. At 12 UTC, as plotted in Fig. 2c (left), the lidar profile was classified as a strong LLJ. At the same time, the ERA5 profile was classified as a transition profile. In general, ERA5 overestimated the wind speed as measured by the lidar by approximately 1.5 m s^{-1}, but in the lower part of the height range swept by the rotor blades, where the lidar observed the presence of the LLJ core, the wind speed was underestimated by
370   up to 1.9 m s^{-1}.

3.4   Validating ERA5 directional shear against lidar observations

In Fig. 8, the distributions and magnitude of the maximum directional shear over the rotor from hourly lidar data and ERA5 data from the same time period, see Fig. 2ab, are plotted for both Östergarnsholm and Utö. The ERA5 residual, insets in Fig. 8a, show similar results for the two sites, overestimating the relative occurrence of minimal directional shear, <2°, and in general
375   underestimating the rest of the distribution. However, for Östergarnsholm, there was a slight overestimation of directional shear in the range 6–12° as compared to the observations. Also in the cumulative distribution, Fig. 8b, it is clear that ERA5 overestimated weak directional shear and underestimated strong directional shear. The total root mean square error (RMSE) was 12.5° for Östergarnsholm and 12.7° for Utö.

Analysing the number of hits (H), false alarms (FA), misses (M) and correct rejections (CR) in terms of ERA5 accurately
380   predicting strong directional shear, >15°, over the rotor at the exact same hour as observed by the lidar measurements, it is clear that ERA5 misses most of the occasions, Fig. 8c). The hit rate, defined as

$$HR = \frac{H}{H + M} \tag{1}$$

was 33% for Östergarnsholm and 32% for Utö. The false alarm rate,

$$FAR = \frac{FA}{H + FA} \tag{2}$$

385   was relatively low for Utö, 4%, but slightly higher for Östergarnsholm, 10%. The frequency bias, defined as

$$FBIAS = \frac{H + FA}{H + M} \tag{3}$$

was 53% for Östergarnsholm and 41% for Utö, signaling that the underestimation of occasions of strong shear was more pronounced at Utö than at Östergarnsholm.

Analysing the BLH from ERA5, Fig. 8c, it is clear for both sites that in general, as expected from Fig. 5, the lidar observations
390   exhibits the highest values of directional shear in stable conditions, i.e., low BLH. Furthermore, it can be seen that ERA5 misses some cases with extremely strong directional shear, although having very low BLH at these time steps and there are cases in ERA5 when the BLH is slightly higher, 300–500 m, resulting in strong directional shear according to the model, while in
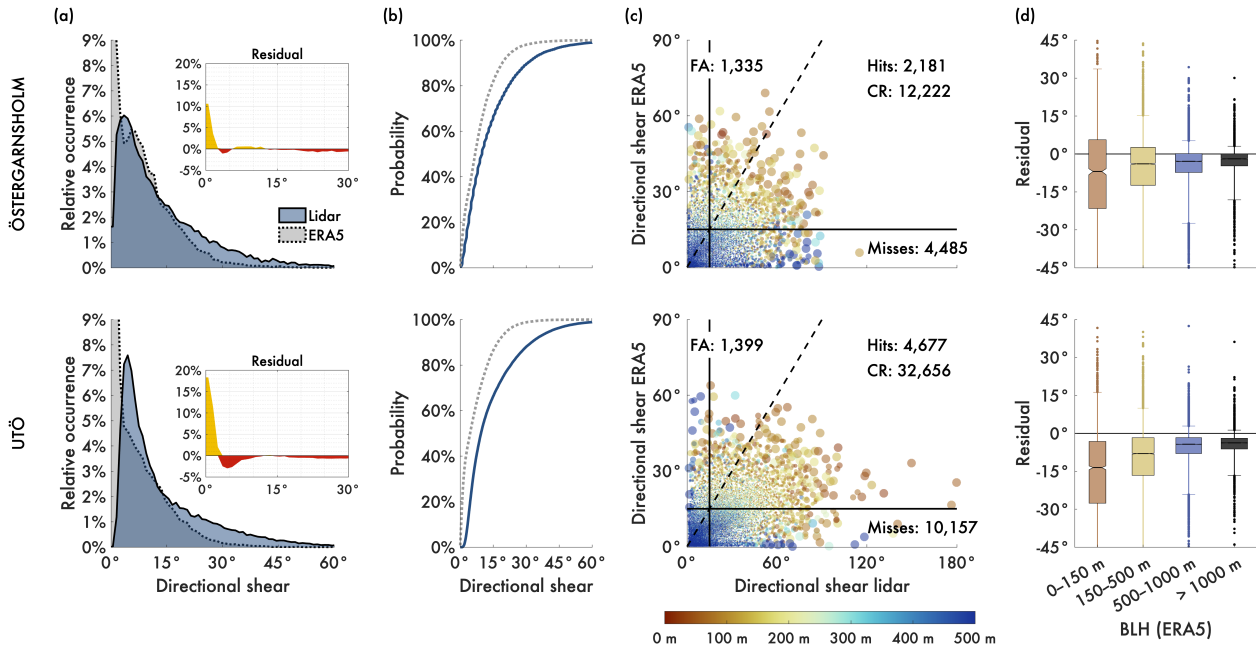
Figure 8. Comparison of directional shear statistics between lidar observations and ERA5 for Östergarnsholm (top row) and Utö (bottom row). In column (a) the relative occurrence of directional shear over the rotor is plotted. Residuals, ERA5 minus lidar, are plotted in the insets. In column (b) the cumulative distributions are plotted and in column (c) the scatter plots of directional shear in ERA5 versus directional shear as measured by the lidar. In the scatter plots, also the number of hits, misses, false alarms (FA) and correct rejections (CR) are given, in terms of ERA5 accurately predicting strong directional shear at the correct time step. In column (c), the ERA5 BLH is indicated by the color coding and the area of each circle is proportional to the inverse of the data density. Solid lines in column (c) mark the 15° threshold for strong directional shear and the dashed line marks the 1:1 ratio. Note the differences on the scales on the abscissa and the ordinate. In column (d), the boxplots show the ERA5 residuals in four classes of BLH (same split as in Fig. 6 a–h). The width of the boxes is scaled with the amount of data in that BLH class. The median of the distributions in each BLH class is marked with a line in the corresponding box and the notches in the box mark the 95% confidence interval of the median. Bottom and top edges of the boxes mark the 25th and 75th percentiles, respectively. Whiskers stretch to the most extreme residual value not considered an outlier and the dots mark data classified as outliers.

reality the directional shear was low, i.e., generating a false alarm. By splitting the BLH into four different classes, it can be seen that ERA5 underestimates the directional shear the most in very low BLH, 0–150 m, with a median underestimation of approximately 14°. As the BLH increases, so does the performance of ERA5, having a median underestimation at Östergarnsholm (Utö) of approximately 6.9° (14°) at 150–500 m BLH, 3.9° (8.0°) at 500–1000 m BLH, 2.9° (4.3°) at 500–1000 m BLH, and 1.9° (3.8°) at BLH larger than 1000 m (all median values for a site significantly different from each other at a 95% confidence level). However, as is illustrated both in panels (c) and (d) in Fig. 8, variations within a BLH class is large and 25% of the data in the lowest BLH class, 0–150 m, exceeds errors of 24° for Östergarnsholm and 28° for Utö.

Table 2. Overview of the percentage of exceedance of thresholds for strong directional shear, 15°, very strong directional shear, 30°, and extremely strong directional shear, 45°, for Östergarnsholm and Utö. The results from the hours of lidar measurements can be directly compared to ERA5 data from the same hours, but also to all hours in the 1979–2021 climatology.

| | Östergarnsholm | | | Utö | | |
	$\geq 15°$	$\geq 30°$	$\geq 45°$	$\geq 15°$	$\geq 30°$	$\geq 45°$
Lidar	32.4%	9.61%	2.73%	31.4%	10.8%	3.16%
ERA5 (same period)	16.9%	1.84%	0.24%	13.0%	1.11%	0.07%
ERA5 (1979–2021)	17.2%	1.95%	0.25%	14.5%	1.14%	0.10%

400   Table 2 accompanies Fig. 8 and shows the relative occurrence of strong, very strong, and extremely strong directional shear respectively for both the lidar measurements and ERA5 from the same time period. In the table, also ERA5 data from the period 1979–2021 is presented for a climatological overview. The relative occurrence of directional shear was much higher in the observations than in the reanalysis, showing the underestimation by ERA5 in all categories. This is also seen in the distributions in Fig. 8a. Numbers are similar between Östergarnsholm and Utö. The relative occurrence of directional shear in
405   the different categories is not perfectly matching between ERA5 for the time period of the measurements and the 1979–2021 climatology, especially for Utö where the relative differences are larger, despite a longer record of observations.

By splitting the data into different categories based on ws150 and wdir150 (Fig. 9), profile type (Fig. 10) and seasonal and diurnal variation (Fig. 11), a comparison of distributions of directional shear between lidar measurements and ERA5 can be performed for subsets of the data. Similar to Fig. 5c, the distribution of directional shear is shifted towards lower values as
410   the wind speed increases, Fig. 9a, both in terms of the median, the 25th and 75th percentiles, the top whisker and the outliers (not all shown in the figure). In all wind speed categories, ERA5 is underestimating the median as well as the 25th and 75th percentiles. For both sites, the most distinct underestimations were seen in the weaker winds. For Östergarnsholm, ERA5 captured the trend of decreasing directional shear with increasing wind speed. However, for Utö, the ERA5 pattern was less clear for the median, but in terms of the 75th percentile, there was a decrease with increasing wind speed. Note that the wind
415   speed at hub height was independently used for the lidar data and the ERA5 data, i.e., at a given time step the wind speed from the observations and from ERA5 could fall into different bins, if there was a mismatch in wind speed.

The analysis of directional shear for different wind directions at hub height, Fig. 9b, also showed a clear underestimation of directional shear for all wind directions, both for Östergarnsholm and Utö. Winds from the south-to-west sector is most common in the Baltic Sea region, and for Utö these wind directions represent a long fetch over open water. For Östergarnsholm
420   however, in westerly winds the air is advected over Gotland before reaching Östergarnsholm and the directional shear could thus have more land-like properties, i.e., in general higher than if the air is advected over the sea, see Fig. 3a. For Östergarnsholm, the median directional shear was also higher, both in observations and in ERA5, for winds from the west, compared to winds from the east. For Utö, winds from the northeast to east sector are most affected by land surfaces, but as Utö is located
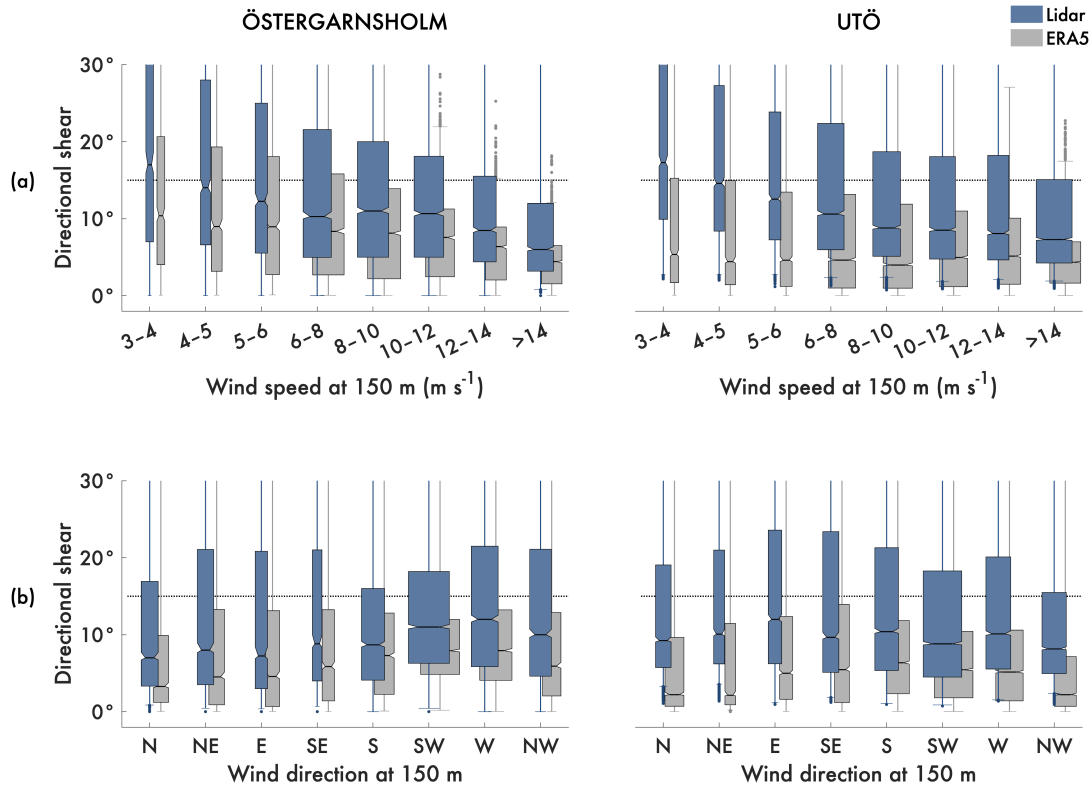
Figure 9. Boxplots of the directional shear in different wind speed at hub height (row a) and wind direction at hub height (row b), comparing lidar measurements with ERA5 for Östergarnsholm (left column) and Utö (right column). The ERA5 data is limited to match the time period of lidar observations, see Fig. 2. The median for each bin is marked with a line in the box and the notches in the boxes mark the 95% confidence interval of the median. Bottom and top edges of the boxes mark the 25th and 75th percentiles, respectively. Whiskers stretch to the most extreme directional shear not considered an outlier and the dots mark data classified as outliers. The dotted horizontal lines mark the 15° threshold that was used for categorizing strong directional shear. The width of the boxes is scaled with the amount of data in the corresponding bin.

far out in the archipelago, the effect is less pronounced than for Östergarnsholm. However, as these wind directions are the least

425   common in the region, Fig. 9b, it is not thought to have a major impact on the overall results. For Östergarnsholm, a detailed analysis of wind profile conditions for different wind sectors can be found in Hallgren et al. (2022).

When analysing the different types of wind profiles, defined in Sect. 2.4, there was an indication of increased directional shear for all types of non-ideal profiles, Fig. 10. ERA5 captured this behaviour, although still underestimating the directional shear. For LLJs, the lidar observations suggest that, in general, the more pronounced the local maximum in the wind speed

430   profile, the stronger the directional shear. Note however that the availability of in some of the categories is very low. This is especially true for ERA5 where not enough LLMs occur to be plotted in Fig. 10.
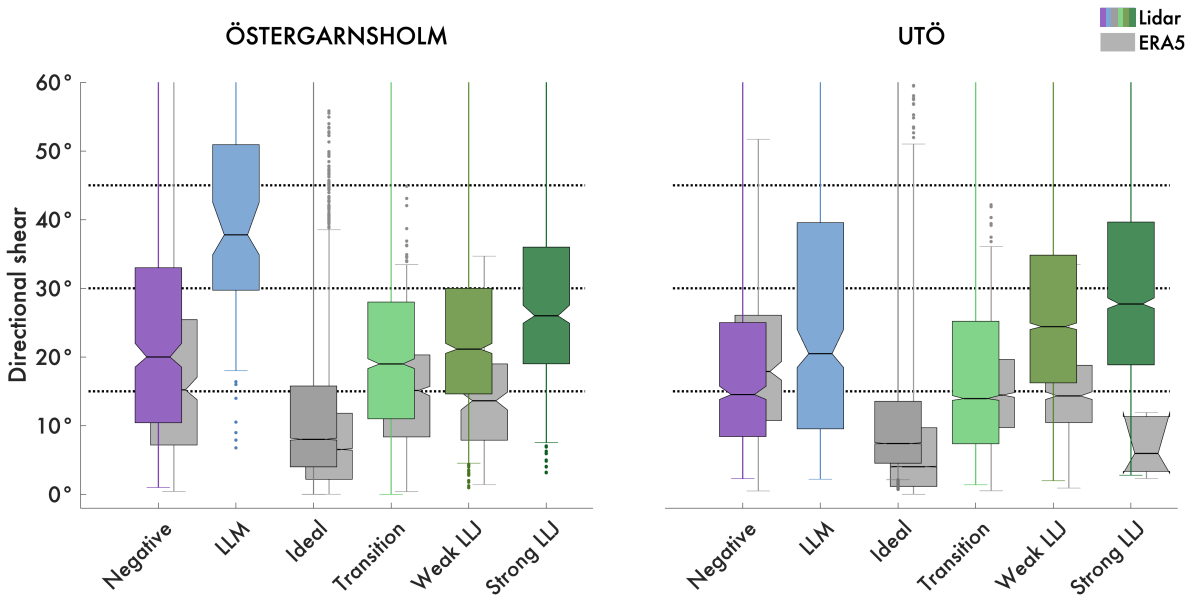
Figure 10. Boxplots of the directional shear in different types of wind speed profiles comparing lidar measurements with ERA5 for Östergarnsholm (left column) and Utö (right column). The ERA5 data is limited to match the time period of lidar observations, Fig. 2. The median for each bin is marked with a line in the box and the notches in the boxes mark the 95% confidence interval of the median. Bottom and top edges of the boxes mark the 25th and 75th percentiles, respectively. Whiskers stretch to the most extreme directional shear not considered an outlier and the dots mark data classified as outliers. Due to the low relative occurrence of some profile types, the widths of the boxes are not scaled as in Fig. 9. In some cases, LLM for both sites and strong LLJ for Östergarnsholm, the ERA5 boxes are missing because of not enough data. The dotted horizontal lines mark the 15°, 30° and 45° thresholds that was used for categorizing strong, very strong and extremely strong directional shear. For reference, the definitions of the different types of wind speed profiles and the applied colour scheme in row matches with the definition and colours as used in Hallgren et al. (2022).

The pronounced seasonality of directional shear at the coastal sites can be seen in Fig. 11a, compare with Fig. 2ab and Fig. 4. During spring and summer (March to August) the directional shear was generally higher than during fall and winter (September to February). Extremes of directional shear exceeding 60° can occur year-round. As expected from earlier plots, ERA5 underestimates the distribution of directional shear for all months. In addition to the seasonality, there was also a pronounced diurnal cycle, Fig. 11b, of directional shear during spring and summer with typically higher values of the median directional shear at night and lower values during the day. For Östergarnsholm, there were indications that ERA5 captured this diurnal behaviour, but for Utö there was no significant diurnal variation. In fall and winter, there was no significant difference in median directional shear throughout the day.
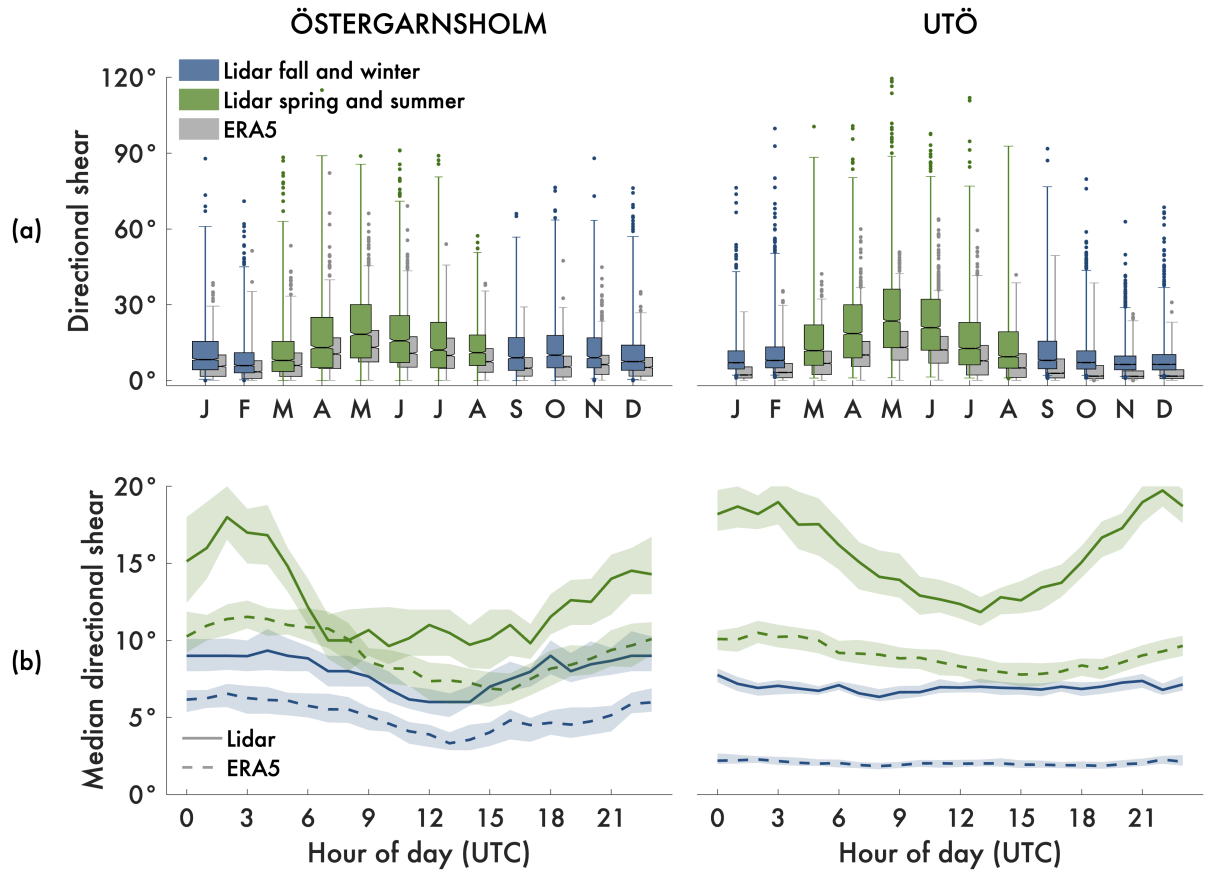
Figure 11. In row (a) the seasonality of directional shear over the rotor for lidar measurements and ERA5 is plotted for Östergarnsholm (left column) and Utö (right column). In row (b), the diurnal change of the median directional shear is plotted for the fall and winter (September to February) seasons and the spring and summer (March to August) seasons. The shaded area around the lines mark the 95% confidence interval of the median. The ERA5 data is limited to match the time period of lidar observations, Fig. 2. In row (a), the median for each month is marked with a line in the box and the notches mark the 95% confidence interval of the median. Bottom and top edges of the boxes mark the 25th and 75th percentiles, respectively. Whiskers stretch to the most extreme directional shear not considered an outlier and the dots mark data classified as outliers. The width of the boxes is scaled with the amount of data in the corresponding month. Note the different scales on the ordinate for row (a) and row (b).

4 Discussion

440

As mentioned in Sect. 1, changes in wind direction over the height range swept by wind turbine blade can be due to many different causes, and it is also evident from the analysis that there is both a pronounced spatial, Fig. 3, and seasonal, Fig. 4, variation of the relative occurrence of cases with strong directional shear. A separation of a lower and upper layer of the air with different properties within the lowest 300 m of the atmosphere, i.e., over the rotor swept by the turbine, seems to be the

445 key factor for establishing strong directional shear, as shown in the analysis of predictor importance at Östergarnsholm and

Utö, Fig. 5ab. Following this, the spatial variation of the BLH between seasons, Fig. 6a–h, seems to be the main explanation of higher occurrence of strong directional shear over land in fall and winter, but higher occurrence of strong directional shear over the Baltic Sea in spring and summer. Furthermore, this is also related to the general wind speed conditions, with generally weaker winds in spring and summer as compared to fall and winter (Fig. 6, see also Fig. 5c). Mesoscale phenomena affecting

450 the winds in the lowest hundreds of meters in the atmosphere, such as the LLJs (Hallgren et al., 2022) which are typically associated with strong stratification of the boundary-layer and sea/land breezes (Hallgren et al., 2023), are also more common at the Baltic Sea coastal areas in spring and summer, contributing to the pronounced seasonality, see Fig. 10 and 11a. The diurnal cycle evident for both Östergarnsholm and Utö during spring and summer in the lidar measurements in Fig. 11b is very likely linked to the generally weaker winds during the evening and night, as the day-time thermally driven convective

455 boundary-layer decreases when the sun sets and vertical mixing decreases.

Differences between the results for Östergarnsholm and Utö are interesting to analyze, and in general Utö was experiencing more cases with strong or extremely strong directional shear, Table 2. While this could be an effect of geographic location, the possible variation in results due to differences in instrumentation should not be underestimated. Although the lidar measurements are considered to be the ground truth in this study, there is an inherent uncertainty in the collected data for both sites, as

460 explained in Sect. 2.2.1 and 2.2.2. For example, as the measurement volume increase with height for the continuous-wave lidar (Östergarnsholm), the profile is also likely to be smoother than measurements performed by a pulsed lidar (Utö). To investigate this variation and possible effect on the results, the Utö lidar profile could be averaged vertically, simulation experiments performed, or a field campaign undertaken with the two types of instruments placed side-by-side for an extended period of time.

465 Since surface friction slows down and turns the wind, it was expected that locations with the highest relative occurrence of strong directional shear were found over land compared to over water, where the surface roughness length is much lower. Furthermore, it was also expected that very strong or extremely strong directional shear typically would occur in complex terrain, i.e., mountainous areas. Katabatic winds, the low-level winds following the downward slope of the terrain, are likely to be the reason for the relatively high number of cases with very strong and extremely strong directional shear along the coast

470 of northern Sweden. As winds from the south to west sector are dominant in the region, the air is typically advected over the Scandinavian mountains and a katabatic air flow is created as the air descends on the other side. The long river valleys from the mountains to the coast also tend to channel the wind, and a separation of the air flow in the lower atmosphere is created, with the terrain-following winds in the lowest layer and the synoptic wind conditions prevailing just a couple of hundred meters higher up. The effect of the valleys can clearly be seen in the ASW LWT maps (supplement) for both seasons, displaying a

475 striped pattern over northern Sweden. Although a bit less pronounced, the channelling by the valleys is also visible in the AS and ASW LWT maps.

In the study by Sanchez Gomez and Lundquist (2020), mentioned in Sect. 1, directional shear exceeding $0.2°$ m^{-1} was not uncommon over Iowa. In the case of the 240 m rotor diameter applied in our study, this would result in a total directional shear of $48°$ if kept over the full rotor. This is more or less directly comparable to Fig. 3c, showing cases with extremely strong

480 directional shear, and keeping the underestimation of 2.5–3 percentage units at Östergarnsholm and Utö in mind, Table 2, we

can conclude that also for Scandinavia and the Baltic Sea, directional shear of similar magnitude also seem to occur quite frequently. The strong seasonality in directional shear observed at the US Atlantic coastal zone by Bodini et al. (2017) matches well with the offshore seasonality over the Baltic Sea that is quantified in this study.

As cases with pronounced directional shear most often occur in rather weak wind conditions, the overall effect on the power
485 production is minor. This is in line with results from Murphy et al. (2020), showing that there was no significant difference in the rotor equivalent wind speed, and thus estimated power production, taking the change in wind direction over the rotor into account for five turbines in the high plains of North America. However, as seen in Fig. 5b, strong directional shear, $\geq 15°$, can occur in wind speeds almost up to 20 m s^{-1} and very strong directional shear, $\geq 30°$, in almost up to 15 m s^{-1}. Since Fig. 5 is purely based on ERA5 data, it is also likely that the distributions should be shifted to be more extreme, following
490 the conclusions from the lidar–ERA5 comparison, e.g., Table 2. Thus, these conditions are needed to be taken into serious consideration, both when constructing new turbines, when forecasting the power production, and when assessing loads on the turbine. Finally, the impact of climate change on primarily the BLH and the general wind speed conditions will be important to be taken into consideration, and it is highly important for the wind energy community that these variables are accurately modeled in climate models.

495 As observed in the numbers in Table 2 and in the distributions in Fig. 8, it is likely that the relative occurrence of directional shear in the three categories (strong, very strong, and extremely strong directional shear) is heavily underestimated by ERA5 in general. This is in line with previous studies showing that NWP models in general suffer in resolving sharp vertical gradients and strong baroclinicity, e.g., Kalverla et al. 2020, and that the mixing profile generally is smoothed to avoid problems with discontinuities in the model. Reducing the turbulent diffusion in stable conditions improves the modeled wind in the boundary-
500 layer Sandu et al. (2013), but deteriorates e.g., both the T2m and the synoptic flow, i.e., the amplitude of the Rossby waves and strength of cyclones and anti-cyclones.

One concern with the ERA5 wind profiles might arise from the fact that the data assimilation can smoothen atmospheric flow due to climatological assumptions in the background error covariances. As we use the analysis data and short forecasts, the data is strongly affected by the data assimilation process. Alternatively, one could use long forecasts or a free-running
505 model, if one is interested in the model climatology of the directional shear and related physical processes. Furthermore, the ERA5 wind direction profile represents an average for the surrounding grid box, which makes the profiles smoother compared to the localized measurements performed by the lidars. This is one of the reasons why the hit rate (Eq. 1, see also Fig. 8c) is so low, and large errors are frequently occurring, similar to the results by Brown et al. 2005; Lindvall and Svensson 2019. It is thus reasonable to think that there is a general underestimation in ERA5 which applies for both offshore, coastal, inland and
510 mountain sites. However, as the validation only was performed at two coastal sites, no bias correction could be applied to the spatial mapping. Future work should employ a large set of lidar measurements covering different terrain and well spread out over the domain to allow for bias correction. For example, onshore measurements from the Finnish lidar network (Hirsikko et al., 2014) could be used for validation. The bias correction could then be implemented in many different ways, but focusing on improving the description of the extreme part of the distribution is high priority to improve assessments on wind turbine
515 loading.

5 Summary and conclusions

Twisting winds affect the power production from a wind turbine as well as from an entire wind farm. Also the longevity of the blades and the turbine are affected due to the difference in alignment of the forces exerted. As a large development of wind power production is expected in northern Europe over the coming decades, a detailed description of the climatological
520 conditions of the wind profile in the region is needed as well as a deeper understanding of physical processes causing extreme cases. As the first study of its kind focusing on the Baltic Sea region, the directional shear over the height interval spanned by the rotor blades of a modern offshore wind turbine was studied in this article, comparing ERA5 reanalysis data to lidar measurements. While it can be concluded that ERA5 underestimates the directional shear for the two coastal sites Östergarns-holm and Utö, it still provides valuable information about the most important predictors, the BLH and the ws150, and that
525 there is a strong seasonality associated with the relative occurrence of strong directional shear.

Furthermore, spatial variation is large, not only comparing onshore and offshore conditions, but also taking the effect of complex terrain, valleys, lakes and forests into account. ERA5 struggles resolving the directional shear, both the general distribution and the extremes, for both Östergarnsholm and Utö and it is important that models are further validated and bias corrected before used for decision making or in operational forecasting of power production or expected turbine loads.

530 **List of acronyms and abbreviations**

BLH Boundary-layer height

ECMWF European Centre for Medium-Range Weather Forecasts

ERA5 ECMWF Reanalysis version 5

IEA International Energy Agency

535 **IFS** Integrated Forecasting System

LCC Low Cloud Cover

Lidar Light Detection And Ranging

LLJ Low-level jet

LLM Low-level minimum

540 **LWT** Lamb Weather Type

NREL National Renewable Energy Laboratory

NWP Numerical Weather Prediction

PCHIP Piece-wise Cubic Hermite Interpolating Polynomial

precip. Precipiation

545 **RMSE** Root Mean Square Error

T2m 2-m temperature

wdir150 Wind direction at hub height

ws150 Wind speed at hub height

Code and data availability. The code used to generate the figures can be acquired by contacting the corresponding author. For the ERA5 data

550 (hourly values on model levels for wind components, temperature, and specific humidity, hourly data on a single-level for surface pressure) we refer to Hersbach et al. (2017). Data were downloaded from the Copernicus Climate Change Service (C3S) (2023). The results contain modified Copernicus Climate Change Service information. Neither the European Commission nor ECMWF is responsible for any use that may be made of the Copernicus information or data it contains.

Author contributions. The project was conceptualized and administrated by CH and ES, with input from HK and SI. Funding acquisition

555 was carried out by ES, HK and SI. The methodology, programming, validation, formal analysis and visualization was performed by CH. CH also wrote most of the original draft, except Sect 2.2.2 (written by VV). CH was supervised by ES, HK and SI. Data curation was performed by ES and VV. All authors participated in reviewing and editing the manuscript.

Competing interests. The authors declare no conflict of interest. The funders had no role in the design of the study; in the collection, analyses, or interpretation of data; in the writing of the manuscript, or in the decision to publish the results.

560 *Financial support.* This research was funded by the Energimyndigheten (Swedish Energy Agency) VindEl program, Grant Number 47054-1. The work forms part of the Swedish strategic research program StandUp for Wind.

Acknowledgements. We acknowledge the use of satellite imagery (Fig. 1a) from the Worldview Snapshots application (https://wvs.earthdata.nasa.gov), part of the Earth Observing System Data and Information System (EOSDIS).

References

Aird, J. A., Barthelmie, R. J., Shepherd, T. J., and Pryor, S. C.: Occurrence of low-level jets over the eastern us coastal zone at heights relevant to wind energy, Energies, 15, 445, 2022.

Arnqvist, J., Segalini, A., Dellwik, E., and Bergström, H.: Wind statistics from a forested landscape, Boundary-Layer Meteorology, 156, 53–71, https://doi.org/10.1007/s10546-015-0016-x, 2015.

Barthelmie, R. J., Shepherd, T. J., Aird, J. A., and Pryor, S. C.: Power and wind shear implications of large wind turbine scenarios in the US Central Plains, Energies, 13, 4269, https://doi.org/10.3390/en13164269, 2020.

Bell, B., Hersbach, H., Simmons, A., Berrisford, P., Dahlgren, P., Horányi, A., Muñoz-Sabater, J., Nicolas, J., Radu, R., Schepers, D., et al.: The ERA5 global reanalysis: Preliminary extension to 1950, Quarterly Journal of the Royal Meteorological Society, 147, 4186–4227, https://doi.org/10.1002/qj.4174, 2021.

Bodini, N., Zardi, D., and Lundquist, J. K.: Three-dimensional structure of wind turbine wakes as measured by scanning lidar, Atmospheric Measurement Techniques, 10, 2881–2896, https://doi.org/10.5194/amt-10-2881-2017, 2017.

Bodini, N., Lundquist, J. K., and Kirincich, A.: US East Coast lidar measurements show offshore wind turbines will encounter very low atmospheric turbulence, Geophysical Research Letters, 46, 5582–5591, https://doi.org/10.1029/2019GL082636, 2019.

Bodini, N., Lundquist, J. K., and Kirincich, A.: Offshore wind turbines will encounter very low atmospheric turbulence, in: Journal of Physics: Conference Series, vol. 1452, p. 012023, IOP Publishing, https://doi.org/10.1088/1742-6596/1452/1/012023, 2020.

Brown, A., Beljaars, A., Hersbach, H., Hollingsworth, A., Miller, M., and Vasiljevic, D.: Wind turning across the marine atmospheric boundary layer, Quarterly Journal of the Royal Meteorological Society: A journal of the atmospheric sciences, applied meteorology and physical oceanography, 131, 1233–1250, https://doi.org/10.1256/qj.04.163, 2005.

Browning, K. and Monk, G.: A simple model for the synoptic analysis of cold fronts, Quarterly Journal of the Royal Meteorological Society, 108, 435–452, https://doi.org/10.1002/qj.49710845609, 1982.

Browning, K. and Wexler, R.: The determination of kinematic properties of a wind field using Doppler radar, Journal of Applied meteorology and climatology, 7, 105–113, https://doi.org/https://doi.org/10.1175/1520-0450(1968)007<0105:TDOKPO>2.0.CO;2, 1968.

Clarke, R.: Observational studies in the atmospheric boundary layer, Quarterly Journal of the Royal Meteorological Society, 96, 91–114, https://doi.org/10.1002/qj.49709640709, 1970.

Copernicus Climate Change Service (C3S): Complete ERA5 global atmospheric reanalysis, https://cds.climate.copernicus.eu/cdsapp#!/dataset/reanalysis-era5-complete, last access: 2023-03-31, 2023.

COWI: Study on Baltic Offshore Wind Energy Cooperation under BEMIP: Final Report; Publications Office of the European Union: Luxembourg, Tech. rep., https://doi.org/10.2833/864823, COWI, Directorate-General for Energy (European Commission), Ea Energy Analyses and THEMA Consulting Group, 2019.

Debnath, M., Doubrawa, P., Optis, M., Hawbecker, P., and Bodini, N.: Extreme wind shear events in US offshore wind energy areas and the role of induced stratification, Wind Energy Science, 6, 1043–1059, https://doi.org/10.5194/wes-6-1043-2021, 2021.

Duffy, A., Hand, M., Wiser, R., Lantz, E., Dalla Riva, A., Berkhout, V., Stenkvist, M., Weir, D., and Lacal-Arántegui, R.: Land-based wind energy cost trends in Germany, Denmark, Ireland, Norway, Sweden and the United States, Applied Energy, 277, 114 777, https://doi.org/10.1016/j.apenergy.2020.114777, 2020.

Ekman, V. W.: On the influence of the earth's rotation on ocean-currents., 1905.

600 Englberger, A. and Dörnbrack, A.: Impact of the diurnal cycle of the atmospheric boundary layer on wind-turbine wakes: a numerical modelling study, Boundary-layer meteorology, 166, 423–448, https://doi.org/10.1007/s10546-017-0309-3, 2018.

Englberger, A. and Lundquist, J. K.: How does inflow veer affect the veer of a wind-turbine wake?, in: Journal of Physics: Conference Series, vol. 1452, p. 012068, IOP Publishing, 2020.

Fernández-Granja, J. A., Brands, S., Bedia, J., Casanueva, A., and Fernández, J.: Exploring the limits of the Jenkinson–Collison weather types
605 classification scheme: a global assessment based on various reanalyses, Climate Dynamics, pp. 1–17, https://doi.org/10.1007/s00382-022-06658-7, 2023.

Foody, R., Coburn, J., Aird, J. A., Barthelmie, R. J., and Pryor, S. C.: Onshore and Offshore Wind Resources and Operating Conditions in the Eastern U.S., Wind Energy Science Discussions, 2023, 1–20, https://doi.org/10.5194/wes-2023-95, 2023.

Gadde, S. N. and Stevens, R. J.: Interaction between low-level jets and wind farms in a stable atmospheric boundary layer, Physical Review
610 Fluids, 6, 014 603, https://doi.org/10.1103/PhysRevFluids.6.014603, 2021.

Gaertner, E., Rinker, J., Sethuraman, L., Zahle, F., Anderson, B., Barter, G. E., Abbas, N. J., Meng, F., Bortolotti, P., Skrzypinski, W., Scott, G., Feil, R., Bredmose, H., Dykes, K., Shields, M., Allen, C., and Viselli, A.: IEA wind TCP task 37: definition of the IEA 15-megawatt offshore reference wind turbine, Tech. rep., National Renewable Energy Lab.(NREL), Golden, CO (United States), https://doi.org/10.2172/1603478, 2020.

615 Gualtieri, G.: Analysing the uncertainties of reanalysis data used for wind resource assessment: A critical review, Renewable and Sustainable Energy Reviews, 167, 112 741, https://doi.org/10.1016/j.rser.2022.112741, 2022.

Hallgren, C., Arnqvist, J., Ivanell, S., Körnich, H., Vakkari, V., and Sahlée, E.: Looking for an Offshore Low-Level Jet Champion among Recent Reanalyses: A Tight Race over the Baltic Sea, Energies, 13, 3670, https://doi.org/10.3390/en13143670, 2020.

Hallgren, C., Ivanell, S., Körnich, H., Vakkari, V., and Sahlée, E.: The smoother the better? A comparison of six post-processing methods to
620 improve short-term offshore wind power forecasts in the Baltic Sea, Wind Energy Science, 6, 1205–1226, https://doi.org/10.5194/wes-6-1205-2021, 2021.

Hallgren, C., Arnqvist, J., Nilsson, E., Ivanell, S., Shapkalijevski, M., Thomasson, A., Pettersson, H., and Sahlée, E.: Classification and properties of non-idealized coastal wind profiles–an observational study, Wind Energy Science, 7, 1183–1207, https://doi.org/10.5194/wes-7-1183-2022, 2022.

625 Hallgren, C., Körnich, H., Ivanell, S., and Sahlée, E.: A single-column method to identify sea and land breezes in mesoscale resolving NWP models, manuscript accepted for publication in AMS WAF, 2023.

Heinemann, G. and Zentek, R.: A Model-Based Climatology of Low-Level Jets in the Weddell Sea Region of the Antarctic, Atmosphere, 12, 1635, https://doi.org/10.3390/atmos12121635, 2021.

Hersbach, H., Bell, B., Berrisford, P., Hirahara, S., Horányi, A., Muñoz-Sabater, J., Nicolas, J., Peubey, C., Radu, R., Schepers, D., Simmons,
630 A., Soci, C., Abdalla, S., Abellan, X., Balsamo, G., Bechtold, P., Biavati, G., Bidlot, J., Bonavita, M., De Chiara, G., Dahlgren, P., Dee, D., Diamantakis, M., Dragani, R., Flemming, J., Forbes, R., Fuentes, M., Geer, A., Haimberger, L., Healy, S., Hogan, R., Hólm, E., Janisková, M., Keeley, S., Laloyaux, P., Lopez, P., Lupu, C., Radnoti, G., de Rosnay, P., Rozum, I., Vamborg, F., Villaume, S., and Thépaut, J.-N.: Complete ERA5 from 1940: Fifth generation of ECMWF atmospheric reanalyses of the global climate. Copernicus Climate Change Service (C3S) Data Store (CDS), https://doi.org/10.24381/cds.143582cf, last access: 2023-03-31, 2017.

635 Hersbach, H., Bell, B., Berrisford, P., Hirahara, S., Horányi, A., Muñoz-Sabater, J., Nicolas, J., Peubey, C., Radu, R., Schepers, D., Simmons, A., Soci, C., Abdalla, S., Abellan, X., Balsamo, G., Bechtold, P., Biavati, G., Bidlot, J., Bonavita, M., De Chiara, G., Dahlgren, P., Dee, D., Diamantakis, M., Dragani, R., Flemming, J., Forbes, R., Fuentes, M., Geer, A., Haimberger, L., Healy, S., Hogan, R., Hólm, E., Janisková,

M., Keeley, S., Laloyaux, P., Lopez, P., Lupu, C., Radnoti, G., de Rosnay, P., Rozum, I., Vamborg, F., Villaume, S., and Thépaut, J.-N.: The ERA5 global reanalysis, Quarterly Journal of the Royal Meteorological Society, 146, 1999–2049, https://doi.org/10.1002/qj.3803, 2020.

640 Hirsikko, A., O'Connor, E., Komppula, M., Korhonen, K., Pfüller, A., Giannakaki, E., Wood, C., Bauer-Pfundstein, M., Poikonen, A., Karppinen, T., et al.: Observing wind, aerosol particles, cloud and precipitation: Finland's new ground-based remote-sensing network, Atmospheric Measurement Techniques, 7, 1351–1375, https://doi.org/10.5194/amt-7-1351-2014, 2014.

Holtslag, A. A. M., Svensson, G., Baas, P., Basu, S., Beare, B., Beljaars, A. C. M., et al.: Stable atmospheric boundary layers and diurnal cycles: challenges for weather and climate models, Bulletin of the American Meteorological Society, 94, 1691–1706,
645 https://doi.org/10.1175/bams-d-11-00187.1, 2013.

Hsu, S.-A.: Mesoscale nocturnal jetlike winds within the planetary boundary layer over a flat, open coast, Boundary-Layer Meteorology, 17, 485–494, https://doi.org/10.1007/BF00118612, 1979.

Janzon, E., Körnich, H., Arnqvist, J., and Rutgersson, A.: Single column model simulations of icing conditions in northern Sweden: Sensitivity to surface model land use representation, Energies, 13, 4258, https://doi.org/10.3390/en13164258, 2020.

650 Jenkinson, A. and Collison, F.: An initial climatology of gales over the North Sea, Synoptic climatology branch memorandum, 62, 18, Meteorological Office, London, U. K, 1977.

Jones, P., Harpham, C., and Briffa, K.: Lamb weather types derived from reanalysis products, International Journal of Climatology, 33, 1129–1139, https://doi.org/10.1002/joc.3498, 2012.

Kalverla, P. C., Steeneveld, G.-J., Ronda, R. J., and Holtslag, A. A. M.: An observational climatology of anomalous wind
655 events at offshore meteomast IJmuiden (North Sea), Journal of Wind Engineering and Industrial Aerodynamics, 165, 86–99, https://doi.org/10.1016/j.jweia.2017.03.008, 2017.

Kalverla, P. C., Duncan Jr, J. B., Steeneveld, G.-J., and Holtslag, A. A.: Low-level jets over the North Sea based on ERA5 and observations: together they do better, Wind Energy Science, 4, 193–209, https://doi.org/10.5194/wes-4-193-2019, 2019.

Kalverla, P. C., Holtslag, A. A., Ronda, R. J., and Steeneveld, G.-J.: Quality of wind characteristics in recent wind atlases over the North Sea,
660 Quarterly Journal of the Royal Meteorological Society, 146, 1498–1515, https://doi.org/10.1002/qj.3748, 2020.

Kettle, A. J.: Unexpected vertical wind speed profiles in the boundary layer over the southern North Sea, Journal of Wind Engineering and Industrial Aerodynamics, 134, 149–162, https://doi.org/10.1016/j.jweia.2014.07.012, 2014.

Kumar, R., Stallard, T., and Stansby, P. K.: Large-scale offshore wind energy installation in northwest India: Assessment of wind resource using Weather Research and Forecasting and levelized cost of energy, Wind Energy, 24, 174–192, https://doi.org/10.1002/we.2566, 2021.

665 Laakso, L., Mikkonen, S., Drebs, A., Karjalainen, A., Pirinen, P., and Alenius, P.: 100 years of atmospheric and marine observations at the Finnish Utö Island in the Baltic Sea, Ocean science, 14, 617–632, https://doi.org/10.5194/os-14-617-2018, 2018.

Lamb, H. H.: British Isles weather types and a register of the daily sequence of circulation patterns 1861-1971, Geophysical Memoirs, 116, London: HMSO, 1972.

Li, H., Claremar, B., Wu, L., Hallgren, C., Körnich, H., Ivanell, S., and Sahlée, E.: A sensitivity study of the WRF model in offshore wind
670 modeling over the Baltic Sea, Geoscience Frontiers, 12, 101 229, https://doi.org/10.1016/j.gsf.2021.101229, 2021.

Lindvall, J. and Svensson, G.: Wind turning in the atmospheric boundary layer over land, Quarterly Journal of the Royal Meteorological Society, 145, 3074–3088, https://doi.org/10.1002/qj.3605, 2019.

Liu, L. and Stevens, R. J.: Effects of atmospheric stability on the performance of a wind turbine located behind a three-dimensional hill, Renewable energy, 175, 926–935, https://doi.org/10.1016/j.renene.2021.05.035, 2021.

675   Mann, J., Peña, A., Bingöl, F., Wagner, R., and Courtney, M. S.: Lidar scanning of momentum flux in and above the atmospheric surface layer, Journal of Atmospheric and Oceanic Technology, 27, 959–976, https://doi.org/10.1175/2010JTECHA1389.1, 2010.

Miller, S., Keim, B., Talbot, R., and Mao, H.: Sea breeze: Structure, forecasting, and impacts, Reviews of geophysics, 41, https://doi.org/10.1029/2003RG000124, 2003.

Murphy, P., Lundquist, J. K., and Fleming, P.: How wind speed shear and directional veer affect the power production of a megawatt-scale
680   operational wind turbine, Wind Energy Science, 5, 1169–1190, https://doi.org/10.5194/wes-5-1169-2020, 2020.

Møller, M., Domagalski, P., and Sætran, L. R.: Comparing abnormalities in onshore and offshore vertical wind profiles, Wind Energy Science, 5, 391–411, https://doi.org/10.5194/wes-5-391-2020, 2020.

Robertson, A. N., Shaler, K., Sethuraman, L., and Jonkman, J.: Sensitivity analysis of the effect of wind characteristics and turbine properties on wind turbine loads, Wind Energy Science, 4, 479–513, https://doi.org/10.5194/wes-4-479-2019, 2019.

685   Rotach, M. W., Andretta, M., Calanca, P., Weigel, A. P., and Weiss, A.: Boundary layer characteristics and turbulent exchange mechanisms in highly complex terrain, Acta Geophysica, 56, 194, https://doi.org/10.2478/s11600-007-0043-1, 2008.

Rubio, H., Kühn, M., and Gottschall, J.: Evaluation of low-level jets in the Southern Baltic Sea: a comparison between ship-based lidar observational data and numerical models, Wind Energy Science, 7, 2433–2455, https://doi.org/10.5194/wes-7-2433-2022, 2022.

Rutgersson, A., Pettersson, H., Nilsson, E., Bergström, H., Wallin, M. B., Nilsson, E. D., Sahlée, E., Wu, L., and Mårtensson,
690   E. M.: Using land-based stations for air–sea interaction studies, Tellus A: Dynamic Meteorology and Oceanography, 72, 1–23, https://doi.org/10.1080/16000870.2019.1697601, 2020.

Sanchez Gomez, M. and Lundquist, J. K.: The effect of wind direction shear on turbine performance in a wind farm in central Iowa, Wind Energy Science, 5, 125–139, https://doi.org/10.5194/wes-5-125-2020, 2020.

Sandu, I., Beljaars, A., Bechtold, P., Mauritsen, T., and Balsamo, G.: Why is it so difficult to represent stably stratified conditions in numerical
695   weather prediction (NWP) models?, Journal of Advances in Modeling Earth Systems, 5, 117–133, https://doi.org/10.1002/jame.20013, 2013.

Seidel, D. J., Zhang, Y., Beljaars, A., Golaz, J.-C., Jacobson, A. R., and Medeiros, B.: Climatology of the planetary boundary layer over the continental United States and Europe, Journal of Geophysical Research: Atmospheres, 117, https://doi.org/10.1029/2012JD018143, 2012.

Shih, Y.-S.: Families of splitting criteria for classification trees, Statistics and Computing, 9, 309–315,
700   https://doi.org/10.1023/A:1008920224518, 1999.

Simpson, J. E.: Sea breeze and local winds, Cambridge University Press, 1994.

Svensson, N., Bergström, H., Sahlée, E., and Rutgersson, A.: Stable atmospheric conditions over the Baltic Sea: model evaluation and climatology, https://helda.helsinki.fi/bitstream/handle/10138/225771/ber21-5-6-387.pdf, 2016.

Svensson, N., Sahlée, E., Bergström, H., Nilsson, E., Badger, M., and Rutgersson, A.: A case study of offshore advection of boundary layer
705   rolls over a stably stratified sea surface, Advances in Meteorology, 2017, https://doi.org/10.1155/2017/9015891, 2017.

Svensson, N., Arnqvist, J., Bergström, H., Rutgersson, A., and Sahlée, E.: Measurements and Modelling of Offshore Wind Profiles in a Semi-Enclosed Sea, Atmosphere, 10, 194, https://doi.org/10.3390/atmos10040194, 2019.

Türk, M. and Emeis, S.: The dependence of offshore turbulence intensity on wind speed, Journal of Wind Engineering and Industrial Aerodynamics, 98, 466–471, 2010.

710   US Department of Energy: Wind turbines: The bigger, the better, https://www.energy.gov/eere/articles/wind-turbines-bigger-better, Retrieved from the Office of Energy Efficiency & Renewable Energy. Last access: 2023-04-17, 2022.

Vakkari, V., O'connor, E., Nisantzi, A., Mamouri, R., and Hadjimitsis, D.: Low-level mixing height detection in coastal locations with a scanning Doppler lidar, Atmospheric Measurement Techniques, 8, 1875–1885, https://doi.org/10.5194/amt-8-1875-2015, 2015.

Vakkari, V., Manninen, A. J., O'Connor, E. J., Schween, J. H., Van Zyl, P. G., and Marinou, E.: A novel post-processing algorithm for Halo Doppler lidars, Atmospheric Measurement Techniques, 12, 839–852, https://doi.org/10.5194/amt-12-839-2019, 2019.

Veers, P., Dykes, K., Lantz, E., Barth, S., Bottasso, C. L., Carlson, O., Clifton, A., Green, J., Green, P., Holttinen, H., et al.: Grand challenges in the science of wind energy, Science, 366, eaau2027, https://doi.org/10.1126/science.aau2027, 2019.

Vimmerstedt, L., Akar, S., Mirletz, B., Sekar, A., Stright, D., Augustine, C., Beiter, P., Bhaskar, P., Blair, N., Cohen, S., et al.: Annual Technology Baseline: The 2022 Electricity Update – Offshore Wind, Tech. rep., National Renewable Energy Lab.(NREL), Golden, CO (United States), https://atb.nrel.gov/electricity/2022/offshore_wind, last access: 2023-04-17, 2022.

Vogelezang, D. and Holtslag, A.: Evaluation and model impacts of alternative boundary-layer height formulations, Boundary-Layer Meteorology, 81, 245–269, https://doi.org/10.1007/BF02430331, 1996.

Wind Europe: Significant developments on offshore wind in the Baltic Sea, https://windeurope.org/newsroom/significant-developments-on-offshore-wind-in-the-baltic-sea/, last access: 2023-04-17, 2021.

Wu, L., Shao, M., and Sahlée, E.: Impact of air–wave–sea coupling on the simulation of offshore wind and wave energy potentials, Atmosphere, 11, 327, https://doi.org/10.3390/atmos11040327, 2020.

715

720

725